STUDIES OF E-BEAM PUMPED MOLECULAR LASERS

R. M. Hill, et al

Stanford Research Institute

Prepared for:

Office of Naval Research
Advanced Research Projects Agency

31 July 1974

The views and conclusions contained in this document are those of the authors and should not be interpreted as necessarily representing the official policies, either expressed or implied, of the Advanced Research Projects Agency of the U.S. Government.

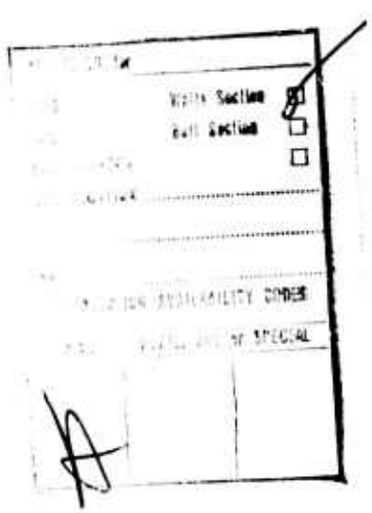

SECURITY CLASSIFICATION OF THIS PAGE (When Dete Entered)

REPORT DOCUMENTATION PAGE

READ INSTRUCTIONS BEFORE COMPLETING FORM

1. REPDRT NUMBER: SRI Number MP 74-39

2. GOVT ACCESSION ND.:

3. RECIPIENT'S CATALOG NUMBER: AD-787079

4. TITLE (and Subtitle): STUDIES OF E-BEAM PUMPED MOLECULAR LASERS

5. TYPE OF REPORT & PERIDD CDVERED: Technical Report No. 3, July 1, 1973 to June 30, 1974

6. PERFORMING DRG. REPDRT NUMBER:

7. AUTHDR(s): R. M. Hill, R. A. Gutcheck, D. L. Huestis, D. Mukherjee, and D. C. Lorents

8. CDNTRACT DR GRANT NUMBER(s): N00014-72-C-0478

9. PERFDRMING DRGANIZATIDN NAME AND ADDRESS: Stanford Research Institute, 333 Ravenswood Avenue, Menlo Park, California 94025

10. PRDGRAM ELEMENT, PRDJECT, TASK AREA & WDRK UNIT NUMBERS:

11. CDNTRDLLING OFFICE NAME AND ADDRESS: Advanced Research Projects Agency, 1400 Wilson Boulevard, Arlington, Virginia 22209

12. REPORT DATE: July 31, 1974

13. ND. OF PAGES:

14. MONITDRING AGENCY NAME & ADDRESS (if diff. from Controlling Dffice): Office of Naval Research, 800 N. Quincy Street, Arlington, Virginia 22217

15. SECURITY CLASS. (of this report): UNCLASSIFIED

15a. DECLASSIFICATION/DDWNGRADING SCHEDULE:

16. DISTRIBUTIDN STATEMENT (of this report)

Distribution of this document is unlimited.

17. DISTRIBUTIDN STATEMENT (of the ebstrect entered in Block 20, if different from report)

18. SUPPLEMENTARY NDTES

19. KEY WDRDS (Continue on reverse side if necessery end identify by block number)

Electron beam
Energy transfer
Molecular laser
Rare gas dimers
Argon
Nitrogen

20. ABSTRACT (Continue on reverse side if necessary end identify by block number)

We describe experimental and theoretical studies which examine the feasibility of attaining laser action in high pressure gas mixtures (in particular Ar + N_2 + NO) excited by electron beam pulses. Using photometrical and photographical means, we have measured 14 reaction rate coefficients for this system, and were able to determine that there exists large populations of metastable excited N_2 (implying long lived high energy storage capacity). A kinetic model program describing the complex interaction of the gases has

DD FORM 1 JAN 73 1473
EDITION OF 1 NOV 65 IS OBSOLETE

Block 20.

been developed which agrees well with experiment. Using this model, we can predict potential laser efficiencies of the following N_2 transitions: an efficiency of almost 1% for the 2+ (0-1) band, 1.8% for the 1+ (0-0) band, and the possibility of efficient lasing in the V-K system.

CONTENTS

ILLUSTRATIONS

TABLES

SUMMARY

The purpose of this program is to develop an understanding of the molecular kinetics pertinent to new high efficiency, high power lasers. We are studying high pressure gases that are initially excited by intense bursts of electrons. This initial pumping energy, which is primarily deposited by creating atomic ions, rapidly collects in the lowest molecular excited state with an overall efficiency for the rare gases near 50%.

Rare gas dimers for which the ground level is repulsive, in particular Xe_2, Kr_2, and Ar_2, have already demonstrated laser action but with disappointing efficiencies. This problem, coupled with the relatively high gain (implying low energy storage capacity) and with vacuum ultraviolet wavelengths, has led us to consider ways of transferring the energy deposited in the rare gas to other gas molecules in order to improve total efficiency, shift the wavelength to the near ultraviolet or visible, and improve the energy storage capacity.

In this report we describe studies of energy transfer in an $Ar + N_2 + NO$ gas mixture. This combination was chosen because many of the reactions have been quantitatively studied and because the nitrogen triplet system of excited states offers good laser candidates as well as a very long-lived metastable state with excellent energy storage potential.

The important results in summary are:

1. Energy from a high energy electron beam can be efficiently transferred into excited states of the rare gases and then transferred to specific excited states of other gases.

2. Three triplet excited states of N_2 [$N_2(C)$, $N_2(B)$, and $N_2(A)$], the sources of second positive, first positive, and Vegard-Kaplan radiations, are all good laser candidates with potential efficiencies between 1 and 10%.

3. Kinetic modeling, coupled with experiments to determine excited state populations and reaction rate coefficients, can lead to the discovery of new laser systems and guide their development.

Measurements were made of the density of the excited N_2 states and their temporal behavior following excitation of the argon. $N_2(C)$ and $N_2(B)$ were monitored by their radiation but the $N_2(A)$ density was determined by adding NO as a tracer. These measurements allowed us to determine a number of reaction rate coefficients which could be combined with others obtained from the literature to construct a kinetic model. The kinetic model computer program included some 32 reactions and had a self-determining time step which reduced the computing time significantly. The results of the model and of the experiments agreed over a wide range of experimental parameters.

The model was used to find optimum conditions of each potential laser state and to predict the expected efficiencies. For the $N_2(C)$ state, the prediction of laser action, efficiency and operating parameters have been confirmed by subsequent work at other laboratories.

BACKGROUND

A considerable effort has been devoted recently to the development of high energy vacuum ultraviolet lasers by pumping high pressure rare gases with electron beams.[1-4] Efficiencies for the conversion of electrical energy into excited electronic states of the rare gases may be as high as 50%. At high pressures this stored energy can be extracted as vuv radiation from the excited rare gas dimers (excimers); moreover, for sufficiently rapid and intense energy deposition, lasing action has been shown to occur on the excimer transitions. Unfortunately, experimental results and more detailed models,[7,8] have indicated that photoionization of the excimers and other processes limit the laser efficiency to about 1%, far less than the earlier expectations of high laser efficiencies that were based on the repulsive nature of the rare gas ground state potentials. In any event, the detailed models[7,8] and the experiments[9] clearly indicate that the excimer levels can be efficiently populated by e-beam pumping under the proper conditions.

We are seeking ways to make use of the efficient and specific energy available in the rare gas excited states to produce laser action in the visible or near uv range. Perhaps the most straightforward approach is to collisionally transfer the excitation directly to another radiating system, atom, or molecule and achieve laser action in these systems. For this approach to be ideal, the transfer rate should be rapid and specific, populating only one or two excited states of the acceptor. These states should be somewhat metastable against radiation and strongly resistant to quenching, and of course the lower level should be unoccupied and strongly quenched by either radiation or collision. We report here observations on electron beam pumped argon, with nitrogen as the main transfer acceptor.

NO was added as a monitor for the metastable $N_2(A^3\Sigma_u^+)$ state, and its properties as a secondary acceptor were determined.

Previous work[10,11] on energy transfer from metastable argon [$Ar(^3P_0)$, $Ar(^3P_2)$] to N_2 has indicated that the triplet states $N_2(C^3\Pi_u)$ and $N_2(B^3\Pi_g)$ are the principal products, while the lowest triplet $N_2(A^3\Sigma_u^+)$ results from subsequent cascade. The pertinent energy levels are shown in Figure 1. Our understanding of the energy flow in e-beam excited pure argon indicates that the path to excimer formation leads through the four low-lying atomic states [$Ar(^3P_2)$, $Ar(^3P_1)$, $Ar(^3P_0)$, $Ar(^1P_1)$]. We expect excitation transfer to occur from these kinetically short-lived atomic states as well as from the excimer levels themselves (as illustrated in Figure 2).

We have monitored the density and time behavior of each of these N_2 states following excitation of the argon by a short, intense pulse of electrons. By varying the argon and nitrogen pressures, we have been able to identify the important reactions and quenching mechanisms, and in several cases we have measured the reaction rate coefficients. Using rate equations for the important species, we have constructed a kinetic model that agrees well with the observed behavior of the excited states. This agreement between model and data over a wide range of pressures and concentrations then allows us to predict potential efficiencies of the various transitions as laser candidates and to suggest the conditions necessary for achieving these efficiencies. The predictions are summarized in Table I.

After our preliminary report of these studies was submitted,[12] Searles and Hart[13] and Ault et al.[14] found lasing action on the N_2 second positive system in e-beam pumped Ar/N_2 mixtures. Their measured efficiencies range from 0.2 to 0.4%.

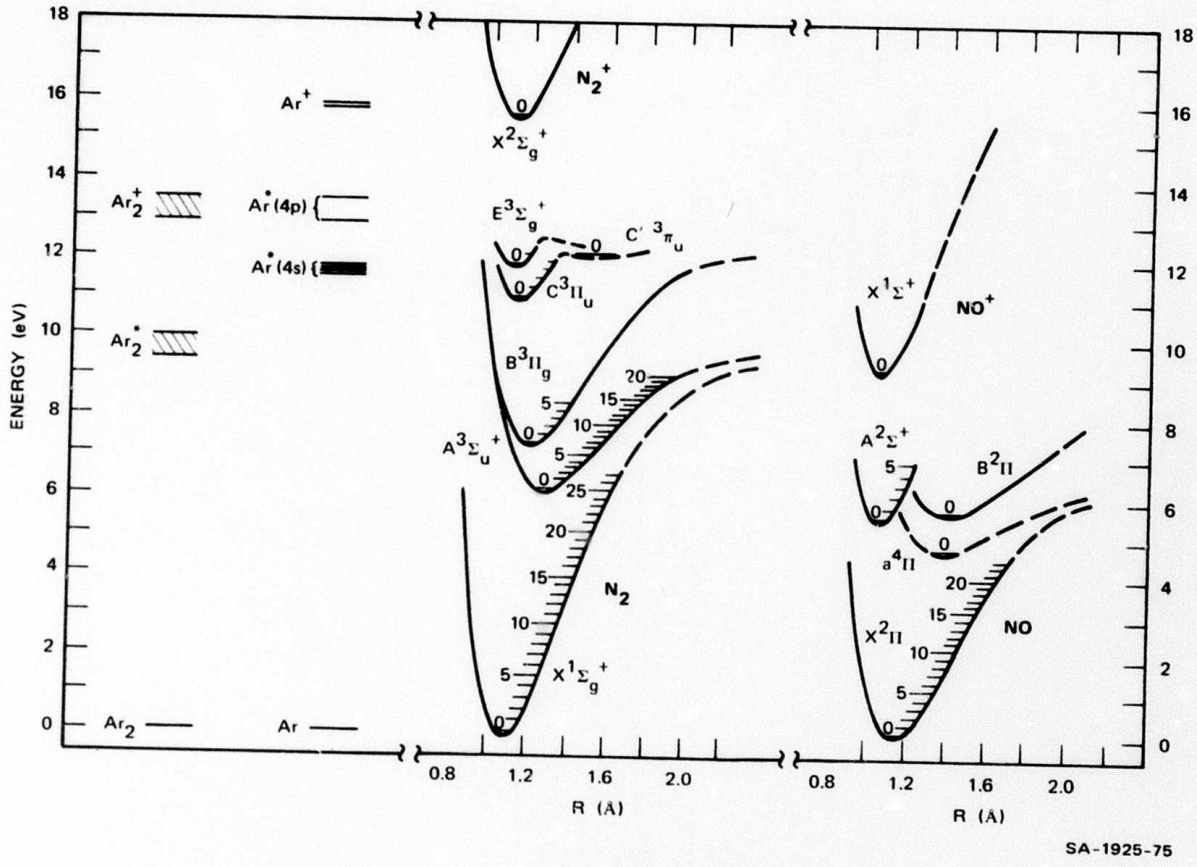

FIGURE 1 SELECTED ENERGY LEVELS FOR Ar, N_2, NO

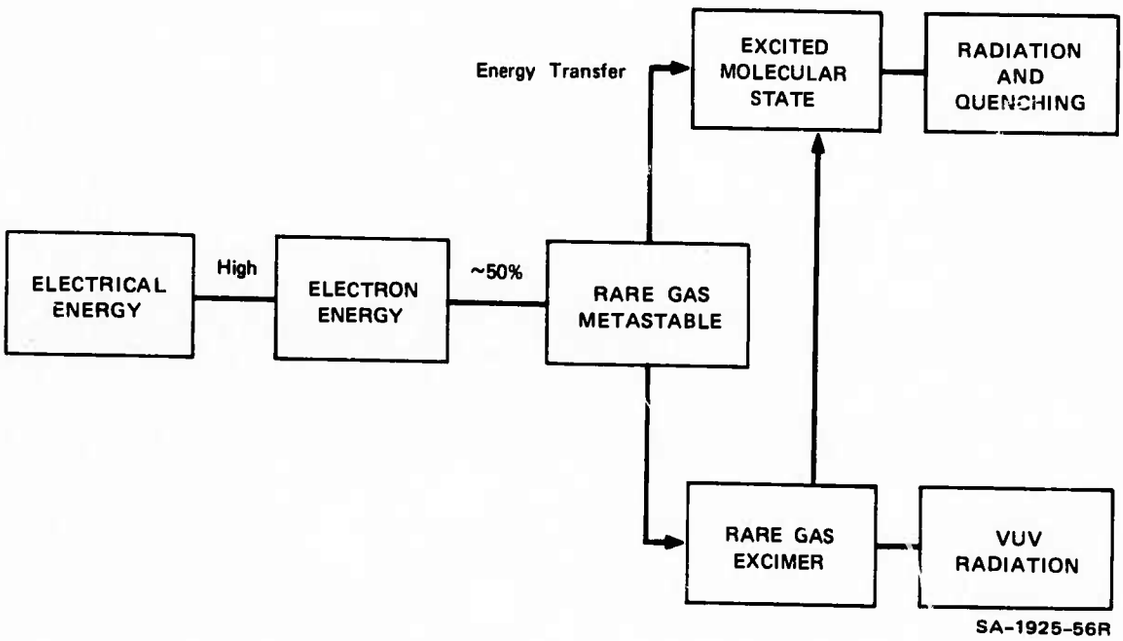

FIGURE 2 ENERGY FLOW AND TRANSFER IN THE Ar-N_2-NO SYSTEM

Table I

POTENTIAL LASER EFFICIENCIES

Upper State	Lower State	Band System	Efficiency
$N_2(C^3\Pi_u)$	$N_2(B^3\Pi_g)$	2+	1%
$N_2(B^3\Pi_g)$	$N_2(A^3\Sigma_u^+)$	1+	1.8%
$N_2(A^3\Sigma_u^+)$	$N_2(X^1\Sigma_g^+)$	V-K	11-22%

APPARATUS AND EXPERIMENTAL PROCEDURE

A schematic diagram of our experimental apparatus is presented in Figure 3. The optical emissions, resulting from the pulsed electron excitation of a gas mixture under high pressure, are viewed by a spectrometer, displayed on an oscilloscope and photographed.

The stainless steel cell used in these mixed-gas studies has a central body containing a cavity 2.5 cm in diameter by 7.5 cm long and sidearms 1.2 cm in diameter by 7.5 cm long. The cell is designed to operate with sample gas pressures between 200 and 10,000 torr (approximately 0.25 to 15 atmospheres). The 1-mil Inconel foil window through which the electron beam enters is tangent to the 1.2-cm aperture of the sidearms to allow viewing along the foil. Windows made of MgF_2 (which are sealed to the sidearms using Teflon gaskets), coupled with the vacuum uv spectrometer, permit observation of spectral emissions from 1300 Å to the infrared.

A Febetron 706 (Hewlett Packard) provides a 2- to 3-nsec, 6000-amp pulse of 600-keV electrons, which passes through about 3 cm of air and then enters the experimental cell through the foil described above. Even after thousands of shots, foil failure has not been a difficulty. Rapid charging and firing (up to 5 shots per minute) was made possible by replacing the charging microswitch with a 1-kΩ resistor.

The cell is surrounded by ¼-inch lead plates to reduce x-ray noise. The residual x-ray pulse is picked up by the photomultiplier and serves as a time calibration.

The optical emissions are viewed through a 0.5-meter monochromator-spectrograph (McPherson model 216.5). Time integrated spectra of the emissions are taken with both Kodak Tri-X (400 ASA) and high speed Polaroid type 57 film (3000 ASA). The band structure and wavelengths

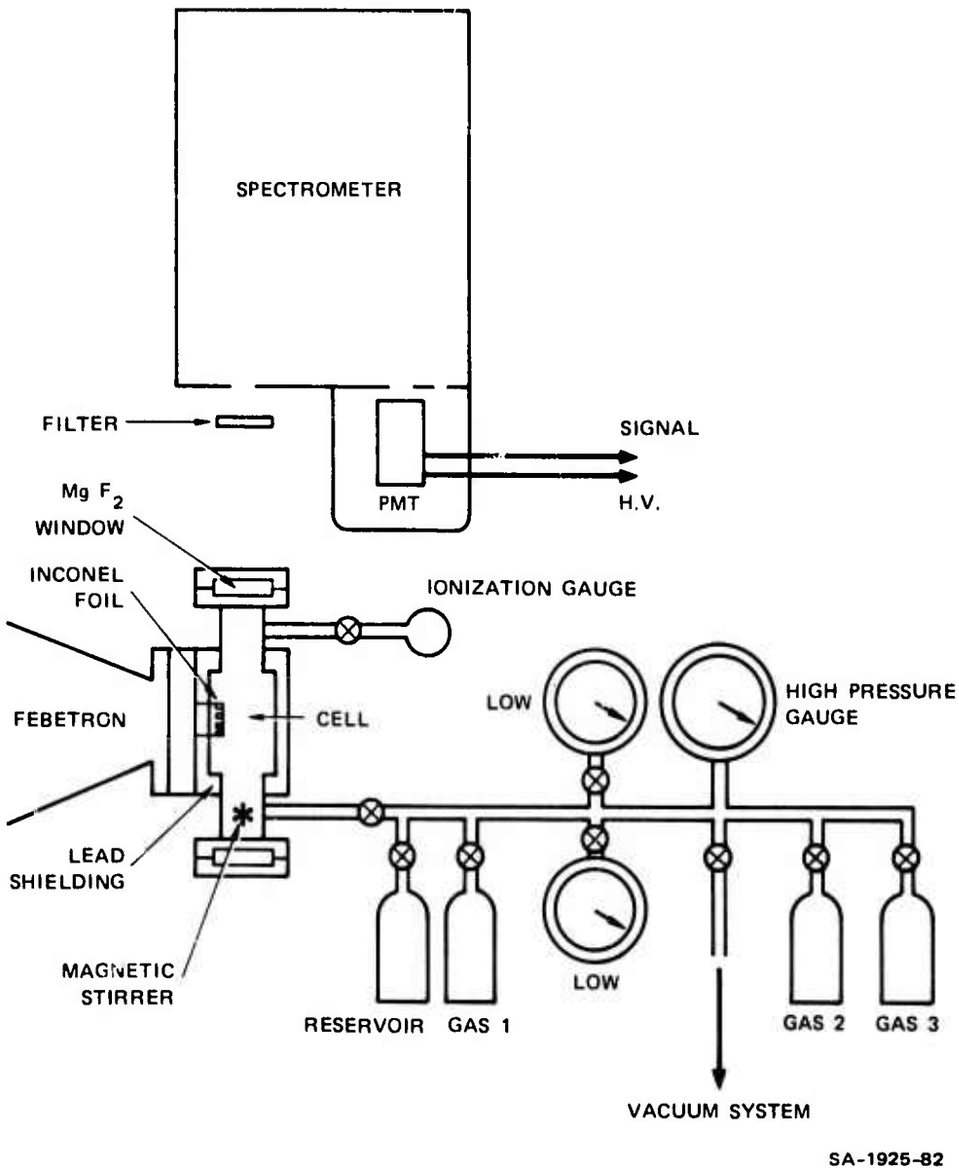

FIGURE 3 SCHEMATIC DIAGRAM OF APPARATUS

are then determined with the aid of either a microdensitometer or a travelling microscope. The temporal behavior of the various emissions is followed by photographing the oscilloscope traces (Tektronix model 485) of individual excitation pulses as detected by a photomultiplier (PMT).

The N_2 first positive band system [$N_2(B^3\Pi_g) \rightarrow N_2(A^3\Sigma_u^+)$, abbreviated 1+ (v'-v")] was initially observed with a filtered photometer having a bandwidth of 200 Å centered at 10,600 Å. This method proved inadequate because the signal was dominated by the bright argon line at 10,469 Å. Consequently, the 1+ (0-0) transition was monitored at 10,421 Å (which eliminated the argon emission), using an RCA 7102 PMT with the monochromator. The 1+ (1-0) emission at 8883 Å was also overlapped by a broad argon excimer band. The narrower 1+ (1-0) feature was observed to appear or disappear with the addition or removal of N_2. The behavior of the Ar_2^* band, which also changed in the appropriate manner with the addition of N_2, was examined by tuning the spectrometer away from the 1+ emission. The short-lived Ar_2^* emission gave a negligible contribution to the longer lived 1+ signal after the first 30 nsec of the afterglow. The 1+ (1-0) transition was thus observed at 8883 Å using a Hamamatsu R-666 PMT, Kodak 35 Wratten filter, and spectrometer.

For the N_2 second positive and NO γ-bands, an S-5 response PMT was used (RCA 1P-28 and Hamamatsu R-666) with the spectrometer. The high intensity of the 2+ emissions at 3371 Å (0-0) and at 3577 Å (0-1) required the use of narrow slits and neutral density filters to prevent saturation of the photomultiplier. Thus, measurements of $N_2(C)$ state production at times late in the afterglow had to be made with a pulsed PMT to obtain sufficient dynamic range while not saturating the tube. The first dynode was pulsed negatively to repel electrons just before the Febetron discharge and was returned to full gain 100 nsec later. On-off ratios in excess of 200 were obtained by this technique.

Detailed comparison with kinetic model calculations (to be described below) required the measurement of the absolute number densities of the emitting species. The optical detection system (monochromator + PMT) was calibrated by using both a tungsten ribbon standard lamp and the molecular branching ratio method.[15] Such a combination, besides providing a means of cross checking the calibration, extended the calibration down to 2400 Å. Appropriately blazed gratings were used with each PMT to ensure maximum sensitivity. For the higher wavelength measurements ($\lambda > 4000$ Å), Kodak Wratten filters were used to eliminate contributions from photons appearing in second order. For the region below 4000 Å, interference filters were used in conjunction with the spectrometer to eliminate the large amount of scattered light that would otherwise have obscured the standard lamp measurements at these shorter wavelengths. Both the N_2 2+ and the NO γ-bands were used for the molecular branching ratio measurements.

The agreement obtained using these methods suggests that our absolute density computations are good to within 60%, the majority of this error being due to our imperfect knowledge of the exact spatial distribution of the emitting species. The relative measurements of different radiating species are expected to be somewhat more accurate; the main uncertainty arises from the use of different PMTs for the different wavelength ranges. For example, the relative measurements of the 1+ and 2+ intensities are believed to be within 40%.

In a kinetic study of this kind, it is not surprising to find that the impurity level in the experimental chamber can affect the temporal behavior of the spectral decays. An ionization gauge installed next to the cell indicated that the residual impurity level in our oil diffusion pump-liquid nitrogen trap vacuum system corresponded to a 0.1-ppm level for gases at 1 atm, much less than the impurity level inherent in the gases themselves. Nevertheless, in searching for Vegard-Kaplan radiation

from N_2, we observed strong emissions from the NO γ-bands. The magnitude of the NO emission was found to be proportional to the number of electron pulses fired into any particular gas sample, leading to the conclusion that the N_2 excited by the pulse was reacting with O_2 that was present as an impurity in the test gas. This impurity caused special concern because transfer to even very small fractions of NO was the dominant loss mechanism for the $N_2(A)$ population at very long times. Indeed the NO γ-band radiation is known to serve as a good tracer of the $N_2(A)$ state population. It was therefore essential to know the NO concentration accurately to obtain reproducible data.

In most subsequent tests small amounts of NO were purposely added to the gas mixture. It was then found that the amount of NO decreased with each excitation pulse. Consequently, after each Febetron shot, the cell was pumped out and a new volume of gas (with a measured admixture of NO) was admitted before the next excitation pulse occurred.

Sample composition was also of concern in the production of the gas mixtures. The mixing time for the minority gases (N_2, NO) with argon was quite long (about a day) at the high pressures used. For each data series, measured amounts of the three gases were combined in a reservoir tank and equilibrated for 24 hours. This reservoir then served as the gas supply to our experimental cell, which could then be filled from 8 to 50 times with the same gas mixture. We also used a small magnetic mixing vane assembly, which rotated inside one arm of the experimental cell when an external magnet was rotated near that arm. Using this system enabled us to decrease the mixing time in the cell from 24 hours to 15 minutes.

DEVELOPMENT OF THE KINETIC MODEL

This investigation, particularly the development of the kinetic model, was founded on our previous work on the processes and kinetics of e-beam pumped rare gases.[5,7] Indeed, a computer code had already been written to describe the rare gas kinetics. The reactions describing the energy flow into and among the states of the added gases were selected largely on the basis of previous kinetic studies of other laboratories.

The reactions used in our mixed gas kinetic model can be divided into four groups. The first of these groups contains the previously studied processes involving the rare gas excitation and ionization and subsequent relaxation to the metastable or excimer levels. The second set describes the transfer of this energy into specific electronic states of the transfer gas, in this case nitrogen. The third set includes the various processes involving these transfer states (quenching, radiation, etc.) and the subsequent buildup of $N_2(A)$ as an energy reservoir. The fourth group of reactions describes energy transfer and decay through the NO, which was added in small but kinetically significant quantities.

The major reactions in each of these four categories are listed in Table II. The flow chart given in Figure 4 summarizes the interactions of these reactions. Those processes involving the initial rare gas excitation have been studied for the excimer laser, and models have been developed by George et al.[8a] and by Lorents et al.[5,7] In the pressure range of interest, 0.5-10 atm, the excitation and the redistribution of the energy into the argon metastable states is very fast compared with most of the other reactions. Indeed, the argon kinetics can be summarized as follows: an instantaneous source of Ar^* becomes Ar_2^* by reaction 3; Ar_2^* then decays by reactions 6 and 7 and by the transfer reactions 8-12,

Table II

MIXED GAS REACTION SYSTEM
($Ar-N_2-NO$)

Reaction No.	Reaction	Rate Coefficient	Reference
	Excitation Reactions		
1	$Ar^+ + 2Ar \rightarrow Ar_2^+ + Ar$	2.5×10^{-31} cm^6/sec	16
2	$Ar_2^+ + e^- \rightarrow Ar^* + Ar$	1×10^{-6} cm^3/sec	17
3	$Ar^* + 2Ar \rightarrow Ar_2^* + Ar$	1×10^{-32} cm^6/sec	18, 19, Measured
4	$Ar^* + Ar^* \rightarrow Ar^+ + Ar + e^-$	5×10^{-10} cm^3/sec	20, Calculated
5	$Ar_2^* + e^- \rightarrow 2Ar + e^-$	1×10^{-9} cm^3/sec	Estimated
6	$Ar_2^* + Ar_2^* \rightarrow Ar_2^+ + 2Ar + e^-$	5×10^{-10} cm^3/sec	Calculated
7	$Ar_2^* \rightarrow 2Ar + h\nu$	2.4×10^{7} s^{-1}	7, 21
	Transfer Reactions		
8	$Ar^* + N_2 \rightarrow$ total	3×10^{-11} cm^3/sec	22, 20, 23, 24, Measured
9	" $\rightarrow N_2(B) + Ar$	1.7×10^{-11} cm^3/sec	10
10	" $\rightarrow N_2(C) + Ar$	3×10^{-12} cm^3/sec	10, 10
11	" $\rightarrow N_2(E) + Ar$	1×10^{-11} cm^3/sec	Estimate
12	$Ar_2^* + N_2 \rightarrow N_2(B) + 2Ar$	1×10^{-11} cm^3/sec	Estimate
	N_2 Triplet Reactions		
13	$N_2(E) + Ar \rightarrow N_2(C) + Ar$	3×10^{-12} cm^3/sec	Estimate
14	$N_2(C) \rightarrow N_2(B) + h\nu$	$2.2\times10^{+7}$ s^{-1}	25, 26, 27, 28
15	$N_2(C) + N_2 \rightarrow N_2(B) + N_2$	1.5×10^{-11} cm^3/sec	25, 29, Measured
16	$N_2(C) + Ar \rightarrow N_2(B) + Ar$	8×10^{-13} cm^3/sec	10, Measured
17	$N_2(B) \rightarrow N_2(A) + h\nu$	1.1×10^{5} s^{-1}	30, 27, 31, 32
18	$N_2(B) + N_2 \rightarrow N_2(A) + N_2$	2.0×10^{-12} cm^3/sec	33, 34, 35, Measured
19	$N_2(B) + Ar \rightarrow N_2(A) + Ar$	4×10^{-15} cm^3/sec	± 34, 30, Measured

Table II (Continued)

Reaction No.	Reaction	Rate Coefficient	Reference
20	$N_2(A)+N_2(A) \rightarrow$ total	1×10^{-10} cm^3/sec	‡ 36, 37, 38, Measured
21	" $\rightarrow N_2(E)+N_2$	1×10^{-11} cm^3/sec	Estimate
22	" $\rightarrow N_2(C)+N_2$	1×10^{-11} cm^3/sec	‡ 37, 39, 40, Measured
23	" $\rightarrow N_2(B)+N_2$	8×10^{-11} cm^3/sec	‡ 26
	NO Reactions		
24	$Ar_2^+ + NO \rightarrow NO^+ + 2Ar$	2.4×10^{-10} cm^3/sec	41
25	$Ar^* + NO \rightarrow$ total	2×10^{-10} cm^3/sec	22, 23
26	$Ar_2^* + NO \rightarrow$ total	7×10^{-10} cm^3/sec	Estimate
27	$N_2(B)+NO \rightarrow$ total	7×10^{-11} cm^3/sec	‡ 34, Measured
28	$N_2(A)+NO \rightarrow$ total	8×10^{-11} cm^3/sec	34, 42, 43, Measured
28a	$N_2(A)+NO \rightarrow NO(A)+N_2$	4×10^{-11} cm^3/sec	‡ 42, 43, Estimate
29	$NO(A) \rightarrow NO(X)+h\nu$	4.5×10^{6} s^{-1}	44, 27, 45, 46, 47
30	$NO(A)+Ar \rightarrow$ total	8×10^{-15} cm^3/sec	‡ 48, 44, Measured
31	$NO(A)+NO \rightarrow$ total	2×10^{-10} cm^3/sec	48, 49, 50

‡ rate coefficient not same as reference--see text.

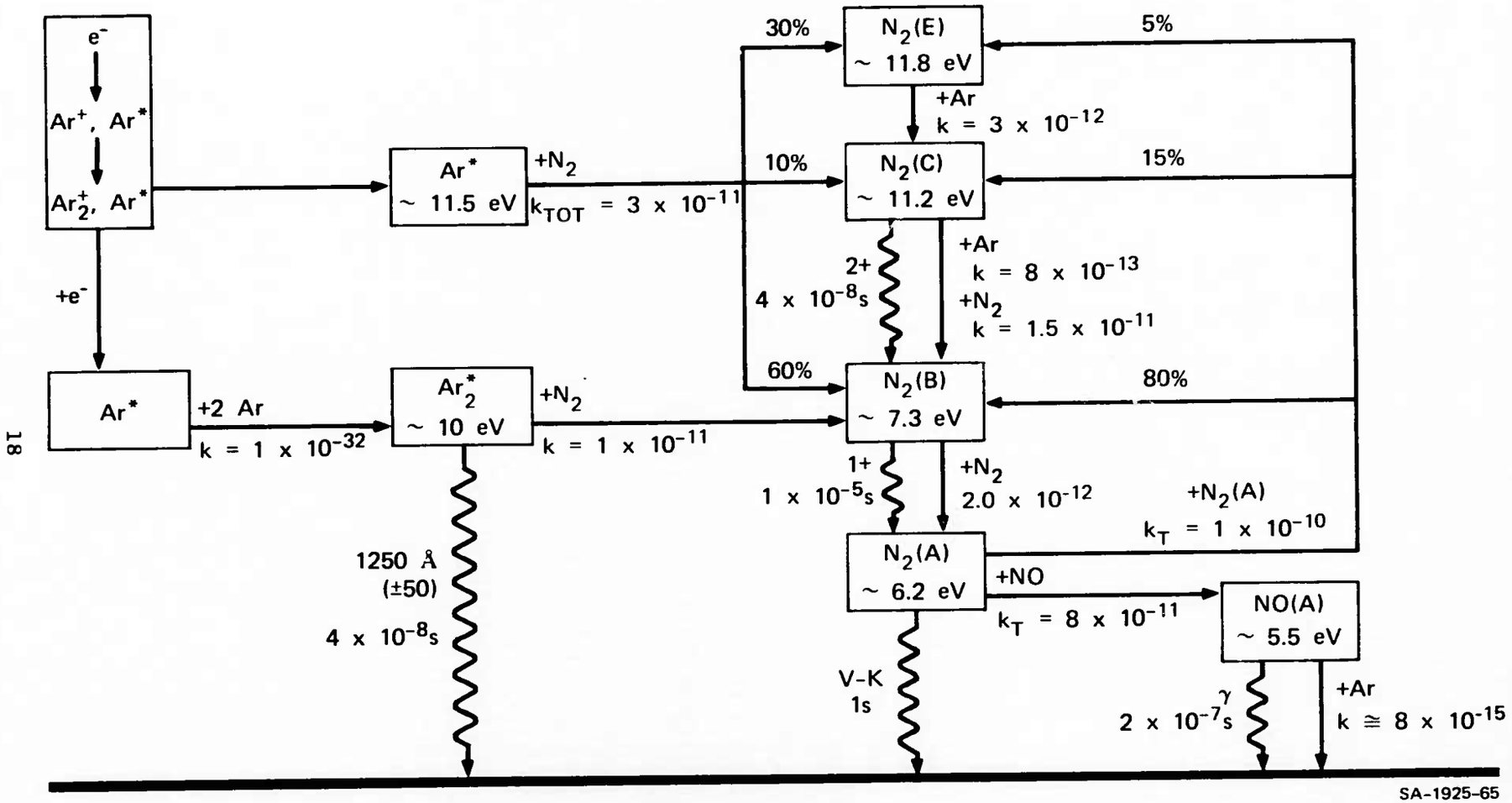

FIGURE 4 DETAILED FLOW CHART FOR THE Ar - N_2 - NO SYSTEM

25, and 26. The efficiency of the energy transfer depends on the relative rate of the transfer reactions and Penning ionization (reaction 6) and radiation (reaction 7). Determination of a definite value for the radiative lifetime of the argon excimer is complicated by the existence of two low-lying molecular states, $^1\Sigma_u^+$ and $^3\Sigma_u^+$, with different radiative transition probabilities. These states can be mixed by collisions with electrons and other atoms to give a lifetime that depends on the excitation conditions. The variation of this lifetime has been treated by Lorents et al.[7] We have chosen to use a single average value, which should be adequate for the pressures and levels of excitation used in the present experiments.

The second section of Table II contains the reactions transferring energy out of the excited rare gas into the N_2 excited states. Several excited atom transfer processes have been studied in low density conditions and the rate constants determined. The rate constant for $^3P_2$ and $^3P_0$ quenching by N_2 seems well established by measurements in several laboratories.[10,20,23,24] The quenching rates of $^3P_1$ and $^1P_1$ have recently been measured by Hurst and coworkers.[51] All these states are produced in the excited Ar, and in the range of pressures and electron densities obtained in our experiment, these states are most likely in statistical equilibrium. We have therefore treated this group of states as a single state that has the mean transfer rate coefficient given for reaction 8.

The disposition of this energy among the states of N_2 is much less clear. Only for the $^3P_{2,0}$ states has there been any detailed examination of the product states,[10] and these results indicate that six $N_2(B)$ states are produced for each $N_2(C)$. Consequently, we have adopted the same ratio in our model, even though this number may be significantly altered by transfer from the $Ar(3p^5 4p)$ levels and perhaps also from $Ar(3p^5 4s\,^1P_1)$. To account for this possibility, we have allowed some transfer into the $(E\,^3\Sigma_g^+)$ state, which can be pumped by the higher Ar^* levels. We also

believe, however, that if $N_2(E)$ is produced, it is quenched rapidly to the C state, which for our range of pressures, is essentially equivalent to allowing the energy to flow directly into the C state. Obviously more work is needed to clarify the energy transfer channels of the higher Ar-N_2 levels.

Our own measurements, discussed in the following section, are consistent with the higher C/B ratio that results from this kinetic picture but provide no direct evidence for the intermediate E state.

Transfer from Ar_2^* to N_2 has not been studied previously. We have estimated a rate constant and specified that all the transfer reactions produce $N_2(B)$ by reaction 12. It is likely that some $N_2(A)$ is produced directly, but it would not be distinguishable from that produced by cascade from $N_2(B)$. Consistency between the kinetic model calculations (to be described below) and the experimental results lends support to this procedure. In any event, except at the very high pressures, little transfer from the excimer actually takes place.

Reactions 13 through 23 in Table II describe the subsequent history of the excited states of nitrogen into which the energy has been transferred. We will begin our discussion at the top of the N_2 level diagram, follow the cascade down to $N_2(A)$, and conclude with the repopulation by A-state pooling.

Collisional quenching by Ar and N_2 dominates the cascade from $N_2(C)$ to $N_2(B)$. The C state quenching by N_2 has a well established rate constant, but the Ar quenching rate was derived from the measurements reported here. The light produced in the $N_2(C)$ 2+ system is certainly intense, but only at quite low pressures does the radiative decay by spontaneous emission compete favorably with the collisional relaxation.

A similar situation occurs for the relaxation of $N_2(B)$ into $N_2(A)$, but here the details of vibrational population will be important for laser application. The electronic quenching of the lower vibrational

states of $N_2(B)$ ($v < 4$) is very much slower than that for the higher vibrational states. In particular the value given by Dryer and Perner[33] for the $N_2(B)$ (v=0) by N_2 is 1.6×10^{-12} cm^3/sec. This value is an order of magnitude smaller than that quoted by Young et al.,[34] which was from studies of higher vibrational levels ($v > 4$). In addition we have quoted our own measured value for the quenching of $N_2(B)$ (v=0) by argon. The literature values are for vibrational levels $v > 3$.

The cascade of these higher N_2 states produces in the end a large population of $N_2(A)$, which serves as the energy reservoir for the late afterglow. The radiative decay and the quenching by ground state N_2 and by argon are essentially negligible, certainly within the time scale of interest to us. The only significant decay mechanisms are energy transfer to NO and mutual destruction in collisions of $N_2(A)$ with another $N_2(A)$.

This pooling reaction has been the subject of study by several research groups, without a satisfactory consensus as to the reaction rate coefficient and its products. The most recent measurement by Hays and Oskam[36,37] gave a rate coefficient of $1.4^{+2.2}_{-0.65} \times 10^{-9}$ cm^3/sec and a specific value of $2.6^{+2}_{-1.4} \times 10^{-10}$ cm^3/sec for $N_2(C)$ as the product. Stedman and Setser[39] and Zipf[40] give 2×10^{-11} cm^3/sec for $N_2(C)$ production, and Zipf[38] derived a value of 3×10^{-10} cm^3/sec for the total $N_2(A)$ self-destruction rate coefficient. This reaction is difficult to follow experimentally since the $N_2(A)$ state cannot be easily observed directly. The situation is further complicated by the possible dependence of the reaction rate coefficient on the vibrational quantum number. Recent measurements of the vibrational relaxation of $N_2(A)$ by N_2 have been made by Dreyer and Perner[52] and by Brennen et al.[53] The rate coefficients are quite small and vary from 3.4×10^{-16} cm^3/sec for v=1 to 3.2×10^{-13} cm^3/sec for v=5.

The previous measurements of A-state pooling were made at low pressures, and the possible incomplete vibrational relaxation may explain the diversity of pooling rate coefficients. Nevertheless, for the higher

pressures of interest to us, most of the $N_2(A)$ population is probably in the v=0,1 vibrational levels, although this is far from certain. We have not included vibrational quenching of $N_2(A)$ in the kinetic model. The A-state pooling rate coefficient we have used was derived from our measurements as discussed in the following section.

The last set of reactions in Table II (24-31) involves the use of NO either as a monitor for the $N_2(A)$ state or as a potential acceptor gas in its own right. The transfer coefficient from $N_2(A)$, $[k_{28}]$, seems to be well established,[34,42,43] and we have independently measured its value several times in the course of our experiments. One should note that the rate of destruction by NO(A) by NO, $[k_{31}]$, is a factor of 3 larger than the transfer coefficient that produces the NO(A) from $N_2(A)$. This rate of destruction places a severe limit on the peak population of the NO(A) that can be achieved, since any effort to increase this population by increasing the amount of NO added to the mixture also increases the rate at which NO(A) is destroyed.

The intensity of the NO(A) γ-band emissions has been used to monitor the $N_2(A)$ population. The reliability of this procedure is sensitively affected by assumed values of the transfer efficiency from $N_2(A)$ to NO(A) and by the quenching coefficient of NO(A) by argon. Callear and Wood[42] suggested a transfer efficiency of 100%, based on various assumptions, including a dubious value for the argon quenching coefficient. Young and St. John[43] gave an efficiency of 75% with rather large error bars. A significant error in estimating these important reactions would affect our value of the $N_2(A)$ density and therefore our value of the pooling rate coefficient. In the following sections we will use our experimental observations and model calculations to put limits on these effects.

EXPERIMENTAL RESULTS

The mixtures of argon, nitrogen, and nitric oxide varied in total pressure from 250 to 7500 torr. The N_2 percentage was varied between 0.1% and 10%, and NO was added at 1 to 10^3 ppm concentration. Bright emissions, listed in Table III, were observed in the N_2 1+, 2+, and NO γ-band systems. Emissions attributable to transitions between excited states of the argon atom and argon dimer were observed weakly at various wavelengths. Each of the N_2 and NO band systems was monitored at various vibrational transitions, both to follow the various vibrational populations and to provide consistency checks for our calibration and analysis.

The observations of the $N_2(C)$ state were made primarily on the 0-0 transition at 3371 Å. Periodic observation of other transitions with $v'=1,2$ indicated vibrational populations in the ratios of approximately 50:5:1 for the first three levels. The three levels showed similar temporal behavior. Film spectra of the second positive emission as well as photomultiplier observations supported the conclusion that the rotational temperature of the N_2 was quite low. The bandwidth for the 0-0 transition was approximately 6-8 Å, strongly peaked on the low frequency end. Photomultiplier observations across the bandwidth appeared to indicate a small amount of rotational heating, especially at the higher gas pressures. One may conclude that most of the radiation comes from $N_2(C)$ molecules nearly in local thermal equilibrium with the ambient gas.

For the $N_2(B)$ state, most of the observations were made on the 0-0 transition near 1.04 microns. Observations of the $v'=1$ level showed a population down by a factor of 50 to 80 with some evidence of continuing vibrational relaxation, as described below. The bandwidth of the 0-0 transition could not be photographed directly as in the case of $N_2(C)$

Table III

TRANSITION WAVELENGTHS

System	Transition	Wavelength (Å)
N_2 2+	0-0	3371
	0-1	3577
	0-2	3805
	1-0	3159
N_2 1+	0-0	10469
	1-0	8883
NO γ	0-2	2470
	0-3	2586
	0-4	2712

above, but was measured by scanning the photomultiplier tube across the band. The half-width (FWHM) for this transition was approximately 120 ±15 Å.

Determinations of the $N_2(A)$ density were made indirectly by monitoring radiation from NO γ-bands when NO was added in relatively small concentration. Most of our observations were made on the 2470 Å 0-2 band or the 2713 Å 0-4 band. Film spectra again showed the rotational temperatures of the double headed bands to be quite low. We estimate that the v=1 population was as much as half of the v=0. NO β-band emissions indicated a population in the $NO(B^2\Pi)$ state about 50% of that of $NO(A)_{v=0}$. Several other bands of the γ-band system radiating from the NO(A) state were monitored to check the relative calibration of the optical system, since the branching ratios for a given vibrational level within the NO gamma system are reasonably well known. The results agreed to within 50%.

Figure 5 shows the typical temporal behavior of the populations of the various radiating species. The points were taken from oscilloscope photographs of the time behavior of individual spectral emissions, and the absolute populations were computed from the calibration for that particular transition. We used the dependence of the temporal behavior of each state on pressure and mixture composition to verify our picture of the energy flow and to measure as many rate coefficients as possible. With a few exceptions, excellent agreement was obtained with rate coefficients available in the literature, as summarized in Table IV.

For the purposes of analysis we will consider separately the early times (less than 1 μsec) and late afterglow decay. The early temporal dependence monitors the production of the various radiating species (i.e., from Ar^* transfer) and the cascade of the stored energy down to $N_2(A)$. The final decay follows the destruction of the $N_2(A)$ population by pooling and NO quenching.

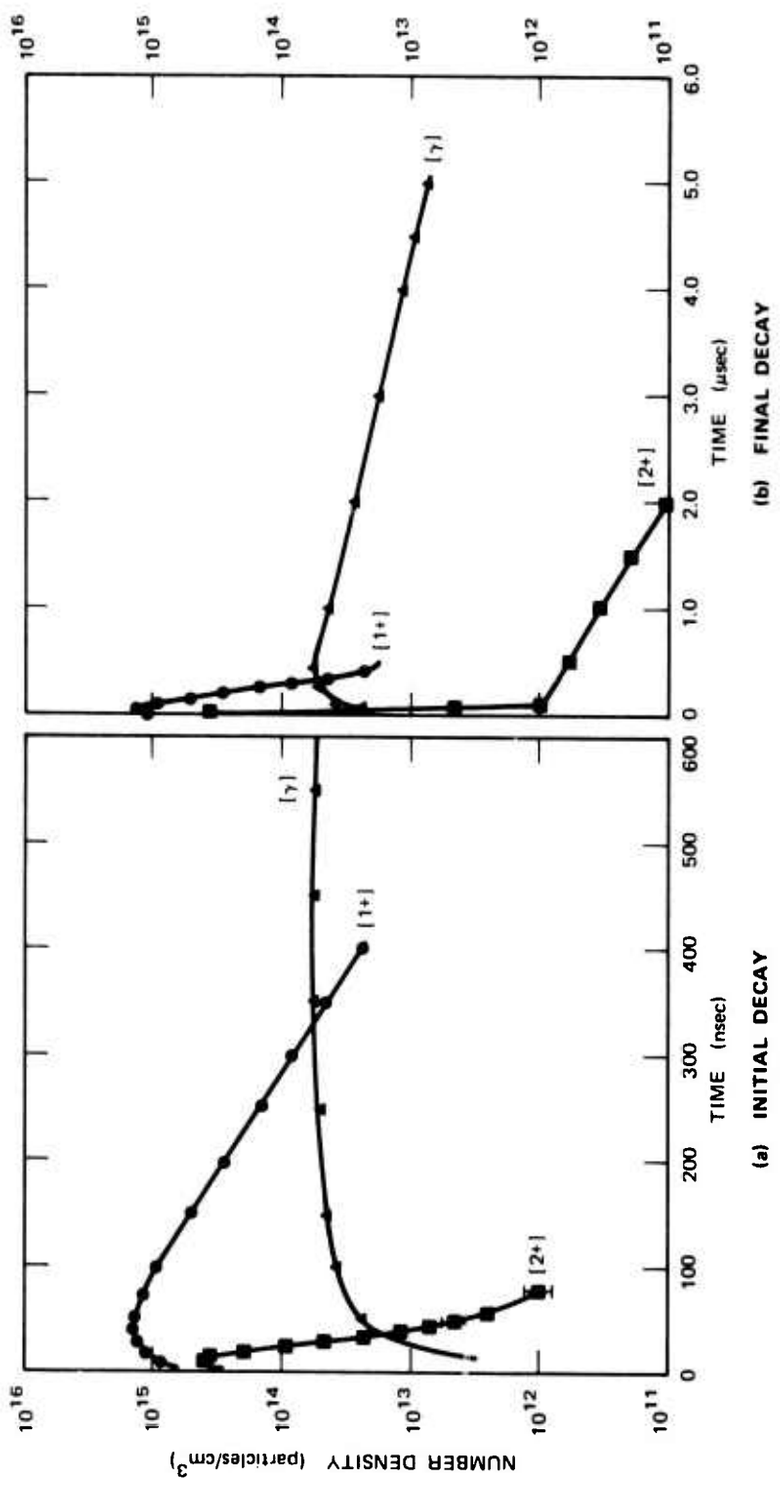

FIGURE 5 TEMPORAL BEHAVIOR OF POPULATIONS AS DETERMINED FROM THE OBSERVED EMISSIONS: 2+ = $N_2(C)$; 1+ = $N_2(B)$; γ = NO(A), FOR A GAS MIXTURE OF 95% Ar, 5% N_2, 0.005% NO AT 3100 torr TOTAL PRESSURE

Table IV

MEASURED RATE COEFFICIENTS

Reaction		Measured Value (cm^3/sec)	Literature Value (cm^3/sec)
$Ar^* + 2Ar$	$Ar_2^* + Ar$	$k_3 = 9.3 \pm 1 \times 10^{-33}$	1×10^{-32}
$Ar^* + N_2$	total	$k_8 = 2 \pm 1 \times 10^{-11}$	3×10^{-11}
$N_2(C) + N_2$	total	$k_{15} = 1.5 \pm .5 \times 10^{-11}$	1.5×10^{-11}
$N_2(C) + Ar$	total	$k_{16} = 5^{+4}_{-2} \times 10^{-13}$	9×10^{-13}
$N_2(C) + NO$	total	$K_{16a} < 10^{-10}$	--
$N_2(B)_{v=0} + N_2$	total	$k_{18} = 1.8 \pm .4 \times 10^{-12}$	1.6×10^{-12}
$N_2(B)_{v=1} + N_2$	total	$K_{18a} = 2.9 \pm .2 \times 10^{-12}$	2.3×10^{-12}
$N_3(B)_{v=0} + Ar$	total	$k_{19} < 5 \times 10^{-15}$	--
$N_2(B)_{v=1} + Ar$	total	$k_{19a} = 1.2 \pm .2 \times 10^{-14}$	--
$N_2(A) + N_2(A)$	total	$k_{20} = 1^{+2}_{-.5} \times 10^{-10}$	3×10^{-10} 1×10^{-9}
$N_2(A) + N_2(A)$	$N_2(C) + N_2$	$k_{22} = 1^{+1}_{-.5} \times 10^{-11}$	2×10^{-11}
$N_2(B)_{v=0} + NO$	total	$k_{27} = 7 \pm 2 \times 10^{-11}$	2.4×10^{-10}
$N_2(A) + NO$	total	$k_{28} = 7.5 \pm 1 \times 10^{-11}$	8×10^{-11}
$NO(A) + Ar$	total	$k_{30} = 8 \pm 3 \times 10^{-15}$	$< 10^{-13}$

The initially produced $N_2(C)$ population disappears as a result of quenching by N_2, $[k_{15}]$, and Ar, $[k_{16}]$. Collisional deactivation by NO is probably rapid but, under our conditions, does not compete with reactions 14, 15, and 16 in Table II. Figure 6 shows the total pressure dependence of the initial exponential decay of the 3371 Å emissions for 5% N_2. By varying the N_2 concentration, we were able to determine the N_2 and Ar quenching rate coefficients: $k_{15} = 1.5 \pm 0.5 \times 10^{-11}$ cm^3/sec and $k_{16} = 5^{+4}_{-2} \times 10^{-13}$ cm^3/sec, respectively. At very low pressures (below 760 torr), we notice that the apparent decay lasts longer than the $N_2(C)$ radiative lifetime (45 nsec). For these N_2 pressures, transfer from Ar^* is slower than the decay of the resulting $N_2(C)$. By studying the concentration dependence of this low pressure decay, we are able to determine the quenching rate coefficients for Ar^*: $k_3 = 9.3 \pm 1 \times 10^{-33}$ (formation of Ar_2^*) and $k_8 = 2 \pm 1 \times 10^{-11}$ (energy transfer to N_2).

Quenching data for the 1+ (0-0) system are shown in Figure 7 for 5% N_2 and various percentages of NO. As before, other curves made with different pressures of N_2 enable us to measure quenching coefficients of the $N_2(B)_{v=0}$ state by all three gases:

$$k_{18} = 1.8 \pm 0.1 \times 10^{-12} \text{ cm}^3/\text{sec} \text{ (by } N_2)$$

$$k_{19} < 5 \times 10^{-15} \text{ cm}^3/\text{sec} \text{ (by Ar)}$$

$$k_{20} = 7 \pm 2 \times 10^{-11} \text{ cm}^3/\text{sec} \text{ (by NO)}$$

The quenching by N_2, $[k_{18}]$ agrees with the recent determination of Dryer and Perner.[33] It is in disagreement with older measurements of Young et al.,[34] but as noted earlier their measurements were determined for vibrational states greater than v=3. We conclude that Young et al. probably measured quenching down the vibrational ladder, whereas our measurements and those of Dryer and Perner were for quenching into other electronic states of N_2. A similar disagreement occurs for the quenching by argon.

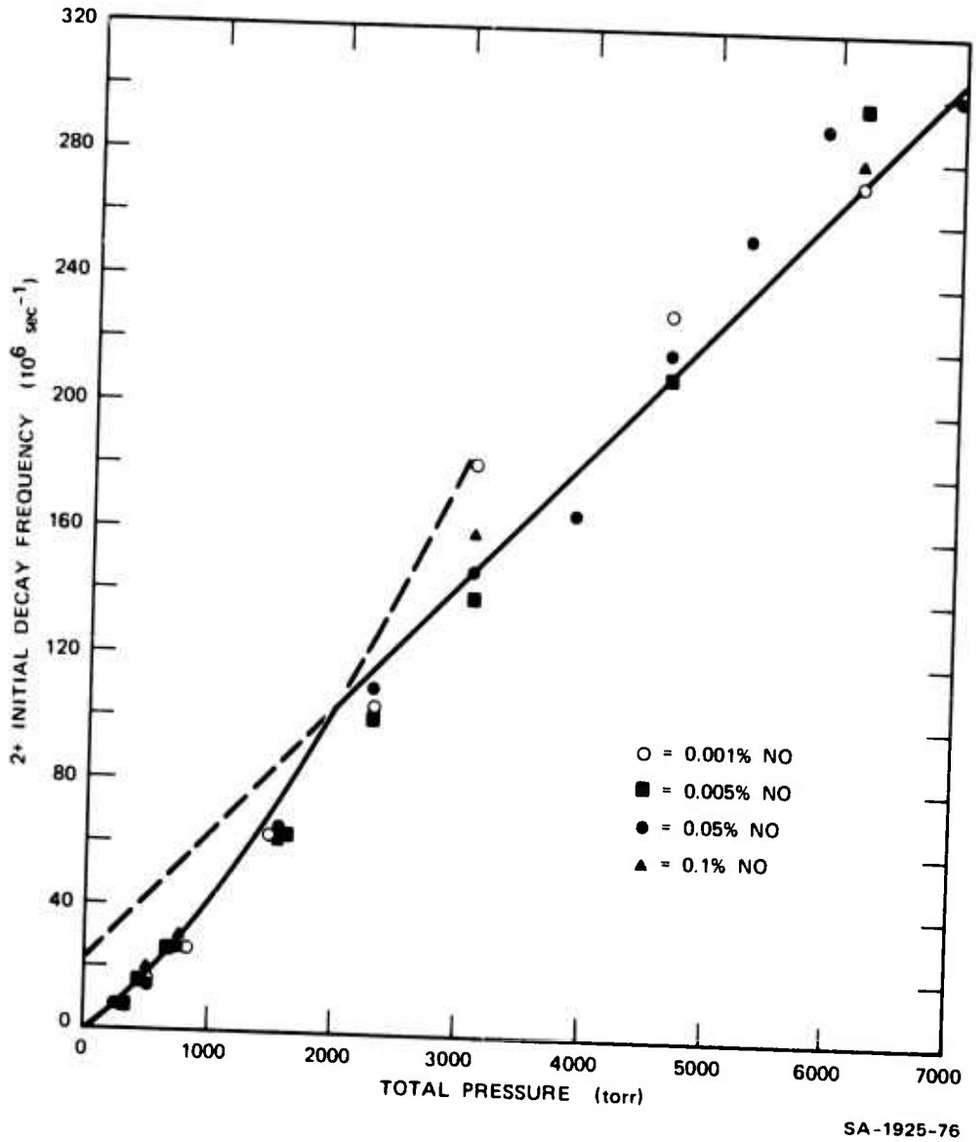

FIGURE 6 INITIAL DECAY FREQUENCY FOR $N_2(C)$ IN MIXTURES OF Ar + 5% N_2 + x% NO

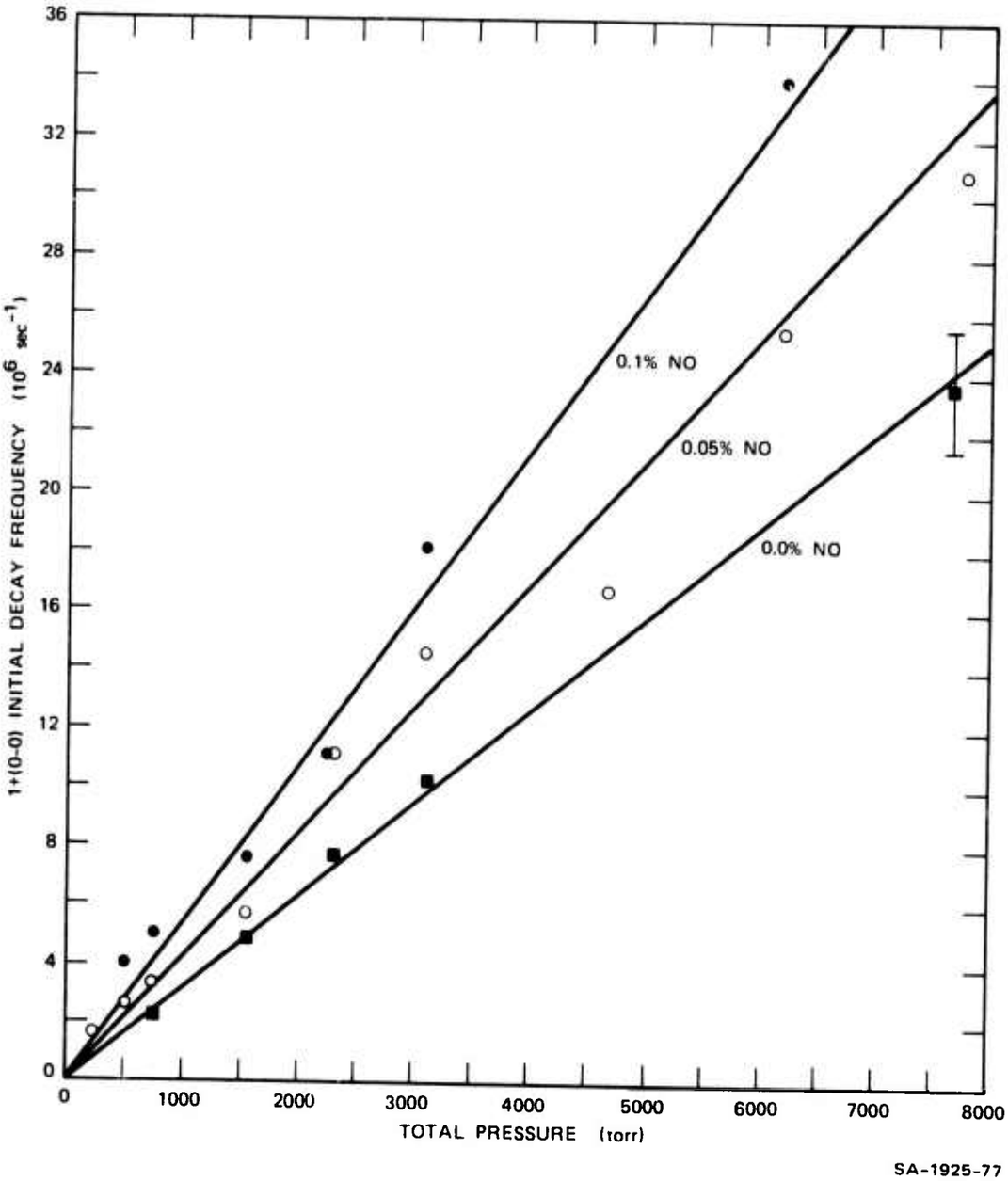

FIGURE 7 INITIAL DECAY FREQUENCY FOR $N_2(B)_{v=0}$ IN MIXTURES OF Ar + 5% N_2 + x% NO

To follow up the distinction between electronic quenching and vibrational relaxation, we studied the pressure dependent temporal decay of the v=1 level of $N_2(B)$. Figure 8 shows the argon and nitrogen dependence of this decay. From these and other similar data, we were able to obtain the v=1 quenching coefficients

$$k_{18a} = 2.9 \pm 0.2 \times 10^{-12} \text{ by } N_2$$

$$k_{19a} = 1.2 \pm 0.2 \times 10^{-11} \text{ by Ar}$$

This vibrational cascade makes no observable contribution to the v=0 population since $v=1/v=0 \simeq 0.02$, but a detailed knowledge of the rate constants is essential for ultimate laser development.

In the later afterglow the decays of the $N_2(C)$ and $N_2(B)$ emissions show the changeover from exponential decay of initial population to a slow nonexponential decay that arises from $N_2(A) + N_2(A)$ pooling. Finally, at low $N_2(A)$ densities, the decay becomes exponential again as energy transfer from $N_2(A)$ to NO becomes the dominant quenching reaction. Since the rapid radiation of the NO(A) state keeps the NO(A) population proportional to that of $N_2(A)$, the NO acts as an effective monitor. Figure 9 shows a plot of the final decay frequency for the NO γ-bands for various concentrations of NO. These measurements had to be made with some care since the NO concentration changed for successive shots into the same mixture; reproducibility was obtained only when a new gas sample was used for each point. Our measured value for the energy transfer from $N_2(A)$ to NO is $k_{28} = 7.5 \pm 1 \times 10^{-11}$ cm^3/sec, in excellent agreement with the literature values cited in Tables II and IV.

Analysis of the nonexponential portion of the late time decay will be facilitated by an examination of the rate equations governing the decay of the various species. At these late times we have an $N_2(A)$ population that decays through reactions 20 and 28:

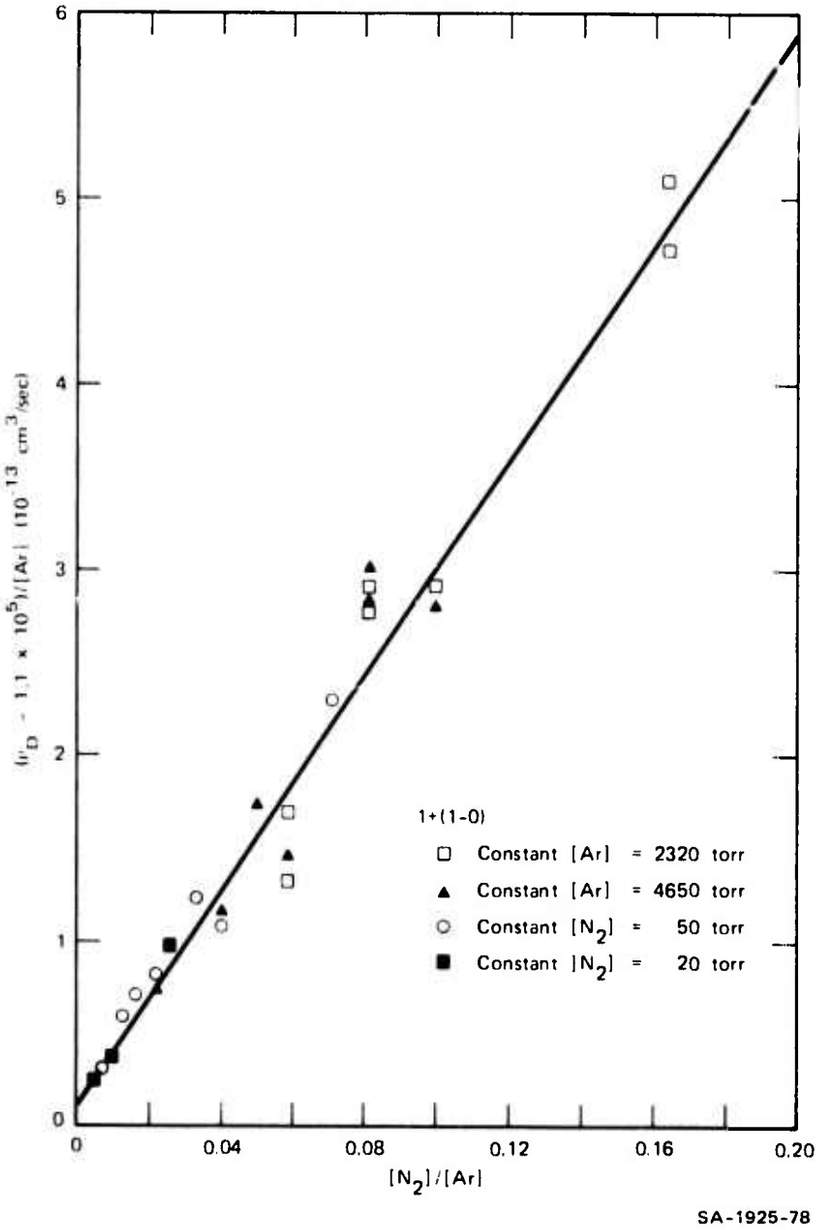

FIGURE 8 INITIAL DECAY OF $N_2(B)_{v=1}$ FOR VARIOUS ARGON AND NITROGEN PRESSURES

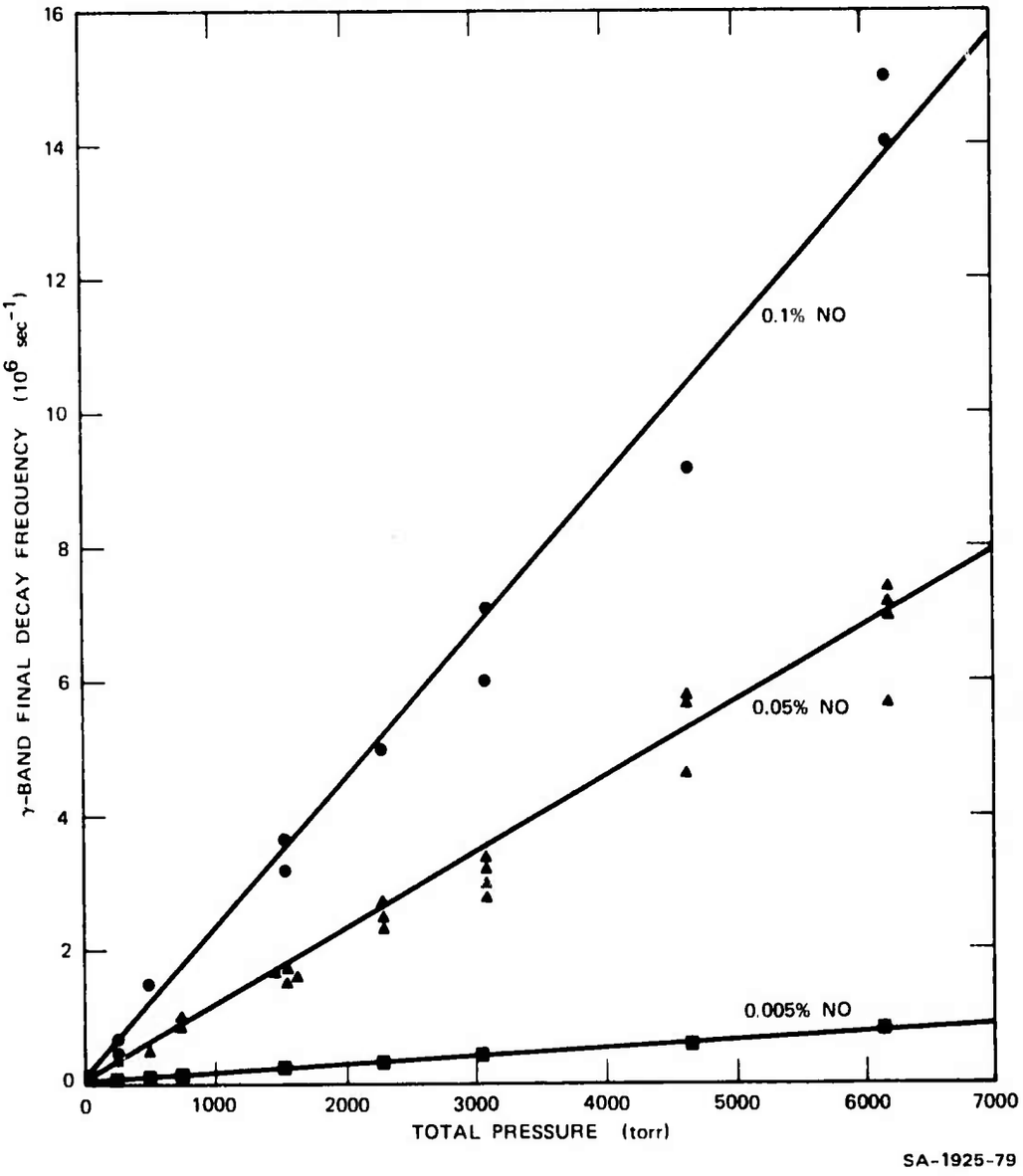

FIGURE 9 NO(A) FINAL DECAY FREQUENCY VERSUS TOTAL PRESSURE
Ar + 5% N_2 + x% NO

$$\frac{d}{dt}[N_2(A)] = -k_{28}[NO][N_2(A)] - k_{20}[N_2(A)]^2 \quad . \tag{1}$$

NO(A) is produced through reaction 28a and relaxed through reactions 29, 30, and 31:

$$\frac{d}{dt}[NO(A)] = -\{k_{29} + k_{30}[Ar] + k_{31}[NO]\}[NO(A)] \tag{2}$$

$$+ k_{28a}[NO][N_2(A)] \quad .$$

Finally $N_2(C)$ is produced and destroyed by reactions 22, 14, 15, 16:

$$\frac{d}{dt}[N_2(C)] = -\{k_{14} + k_{15}[N_2] + k_{16}[Ar]\}[N_2(C)] + \tag{3}$$

$$+ k_{22}[N_2(A)]^2 \quad .$$

$N_2(B)$ obeys a similar equation, but was much more difficult to follow experimentally.

As described previously, each $N_2(C)$ and NO(A) molecule radiates or is quenched very rapidly after it is produced. In the late afterglow the $N_2(C)$ and NO(A) populations remain in kinetic equilibrium with that of $N_2(A)$ and hence serve as monitors of the $N_2(A)$ population through the equations:

$$NO(A) \approx \frac{k_{28a}}{\{k_{29} + k_{30}[Ar] + k_{31}[NO]\}} \cdot [NO][N_2(A)] \tag{4}$$

$$N_2(C) \approx \frac{k_{22}}{\{k_{14} + k_{15}[N_2] + k_{16}[Ar]\}} [N_2(A)]^2 \tag{5}$$

As described in our preliminary report,[12] the $N_2(A)$ temporal behavior is best understood by examining its logarithmic derivative:

$$\frac{\frac{d}{dt}[N_2(A)]}{[N_2(A)]} = -k_{28}[NO] - k_{20}[N_2(A)] \qquad (6)$$

The proportionality of NO(A) and $N_2(A)$ suggests the graph shown in Figure 10. The intercept, at $[NO(A)] \sim [N_2(A)] = 0$, gives the very long time exponential decay frequency $k_{28}[NO]$. Using equations (4) and (6) we find that the slope of $\frac{d}{dt}[NO(A)]/[NO(A)]$ versus NO(A)/NO(X) is given by

$$\text{slope} = \frac{\{k_{29} + k_{30}[Ar] + k_{31}[NO]\}}{k_{28a}} \cdot k_{20} \qquad (7)$$

Measurement of this slope for various argon pressures indicated a dependence much smaller than that suggested by the previous literature values of k_{30}(i.e., $\sim 10^{-13}$). The decay of the γ-band emissions in Ar + NO mixtures gave a more consistent value, $k_{30} = 8 \pm 3 \times 10^{-15}$ cm^3/sec. Our NO γ-band and β-band observations (described above) suggest that the efficiency of the energy transfer from $N_2(A)$ is near 50%. This value is also consistent with our model calculations of the absolute NO(A) density. Using the values $k_{30} = 8 \times 10^{-15}$ cm^3/sec and $k_{28a} = 4 \times 10^{-11}$ cm^3/sec with the known values of k_{29} and k_{31} gives $k_{20} = 1^{+2}_{-0.5} \times 10^{-10}$, in satisfactory agreement with the determination of Zipf.[38]

Absolute calibration of the 2+ emission at late times also permits determination of the specific pooling rate coefficient into $N_2(C)$. Comparison of equations (4) and (5) gives

$$k_{22} = \{K_{14} + k_{15}[N_2] + k_{10}[Ar]\} \cdot \left\{\frac{k_{28a}[NO]}{k_{29}+k_{30}[Ar]+k_{31}[NO]}\right\}^2 \cdot \frac{N_2(C)}{[NO(A)]^2} \qquad (8)$$

A typical graph of the late time $N_2(C)$ and NO(A) number densities is shown in Figure 11. A quadratic dependence is clearly indicated. Insertion of the appropriate rate coefficients gave $k_{22} = 1^{+1}_{-0.5} \times 10^{-11}$ cm^3/sec, again

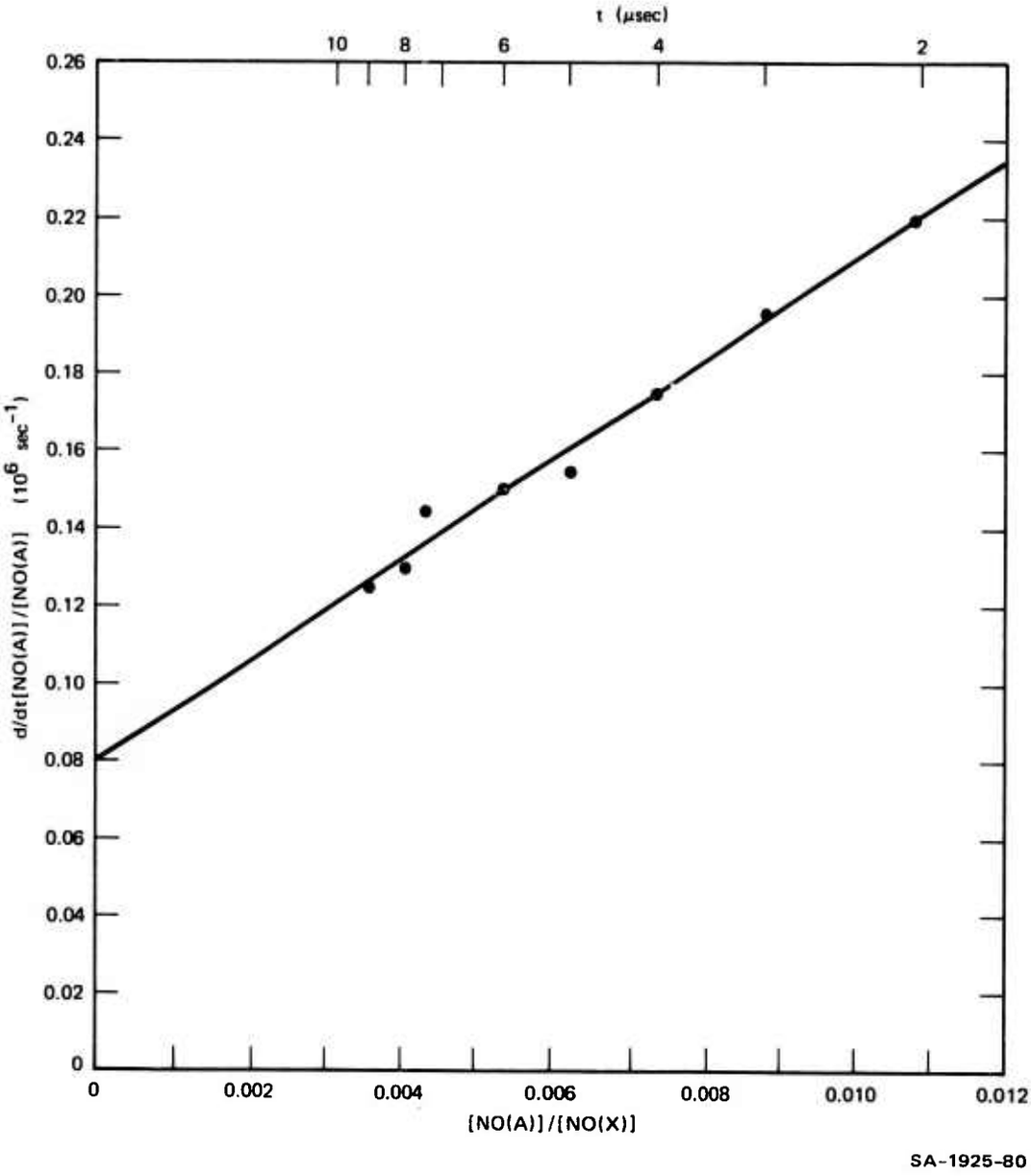

FIGURE 10 LOGARITHMIC DERIVATIVE OF NO γ-BAND EMISSIONS MONITORING $N_2(A)$ DENSITY IN A MIXTURE OF Ar + 5% N_2 + 0.001% NO AT 60 psia TOTAL PRESSURE

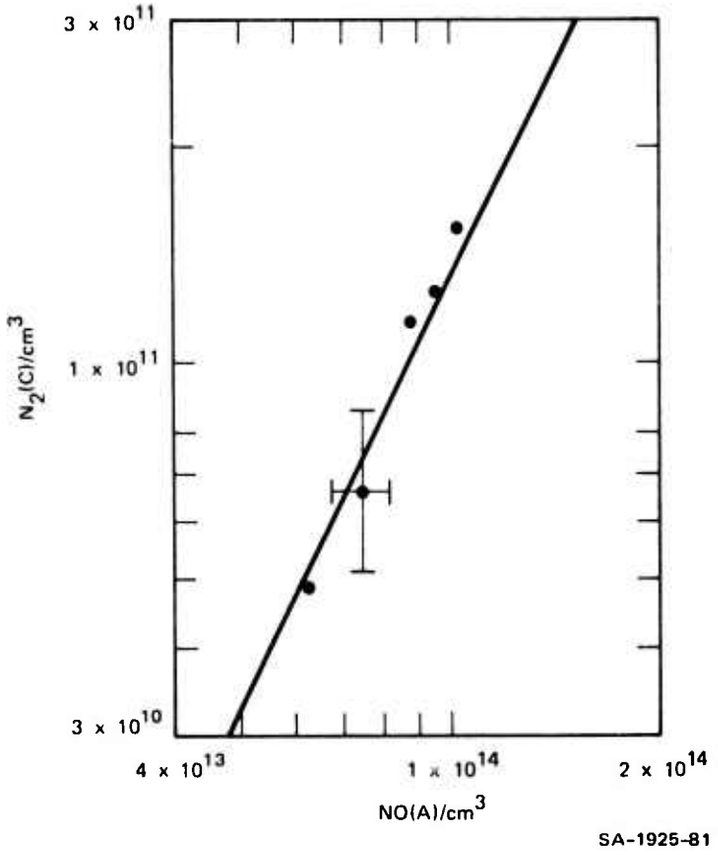

FIGURE 11 QUADRATIC DEPENDENCE OF $N_2(C)$ ON NO(A) IN A MIXTURE Ar + 5% N_2 + 0.005% NO AT 120 psia TOTAL PRESSURE

in satisfactory agreement with the previous work of Stedman et al.[39] and Zipf.[40] Clearly these pooling reactions are difficult to monitor. Special effort will be needed to remove the ambiguities of NO(A) as an $N_2(A)$ state monitor.

COMPUTER MODELING STUDIES

Our previous studies of the rare gas and mercury excimers[5,7,54,12] have indicated the considerable gains in understanding and interpreting experimental results that can be obtained by concurrent numerical modeling of the reaction kinetics. The greater complexity of the mixed gas reaction scheme makes computer modeling even more necessary. Our computer modeling presently includes all the species and reactions in Table II, distinguishing different electronic states separately.

As described above, many of the reactions included in Table II are susceptible to direct experimental study. The most difficult perhaps are those that depend on the reaction of two excited species, since an absolute number density calibration is needed for their study. In computer modeling these reactions, the absolute calibration enters through the choice of the "source" term. We have represented the deposition of energy by the Febetron by a source of ~~8.9~~ 4.4 x 10^{14} Ar^+ ions per cm^3 per nsec per atmosphere and ~~2.5~~ 1.2 x 10^{14} Ar^* excited atoms per cm^3 per nsec per atmosphere for the duration of the 2 nsec Febetron electron pulse. These source terms were at first justified by comparison with deposition codes run at other laboratories and finally by agreement with our absolute measurement of emission intensities.

Computation of the time dependent number densities for a system involving the 31 reactions listed in Table II poses a numerical problem of no mean difficulty. The kinetics of the Ar, N_2, NO mixture during and after e-beam bombardment are modeled by a set of nonlinear, coupled, first-order, ordinary differential equations, which can be symbolically represented by

$$\frac{dy_i}{dt} = f_i(y_1(t), y_2(t), \ldots y_N(t), t) \quad i = 1, \ldots N \qquad (9)$$

Here $y_i(t)$ is the concentration of component i, f_i represents the net effect of all processes affecting y_i, and N is the number of components considered (N = 10 in our model). Given the set of initial conditions, $y_i\ (t=0) = y_i$, i = 1, ... N, it should in principle be possible to integrate equation (9) using a standard procedure such as Runge-Kutta or predictor-corrector. In practice, numerical instabilities are all too frequent.

The concentrations of most of the species studied reach their maximum values during or shortly after the termination of the electron pulse. Subsequently the species decay simultaneously, generally at different rates, but eventually establishing kinetic equilibrium after which they decay at the same or related rates. Examples of this general behavior have been illustrated above; specifically, at late times all significant species are in kinetic equilibrium with the energy reservoir, $N_2(A)$. The speed at which kinetic equilibrium is reached is dominated by the faster reactions [e.g., $Ar^* + N_2$, $N_2(C) \rightarrow N_2(B)$]. The final decay is generally much slower.

Unfortunately, the standard numerical schemes are unstable unless the step-size is chosen according to the fastest reaction rate constant, even if the corresponding species has decayed to quite an insignificant concentration. Large differences in the various reaction rates result in the use of inconveniently small steps (e.g., 10^{-10} sec steps for $N_2(A)$, which may last more than 10^{-5} sec). Not only are such small steps costly but they can cause the accumulation of large round-off errors.

The extent of the disparity of the various rate constants is referred to as the "stiffness" of the reaction system. The remedy for this difficulty can be illustrated by a simple example. The exact solution to the two-species system,

$$\frac{dx}{dt} = \alpha x + \beta y \tag{10}$$

$$\frac{dy}{dt} = \gamma x + \delta y$$

is given by

$$x = \zeta_1 e^{\lambda_1 t} + \zeta_2 e^{\lambda_2 t} \tag{11}$$

$$y = \eta_1 e^{\lambda_1 t} + \eta_2 e^{\lambda_2 t}$$

where λ_1 and λ_2 are the eigenvalues of the decay matrix $\begin{bmatrix} \alpha & \beta \\ \gamma & \delta \end{bmatrix}$, and ζ_1, ζ_2, η_1 and η_2 are constants obtained from the initial conditions. The solution is valid regardless of the disparity of the rate constants. In general, for nonlinear systems such as equation (9), the local decay rates are given by the eigenvalues of the Jacobian decay matrix $\partial f_i / \partial y_j$. A local solution may then be obtained by transforming the kinetic equations to equations over the eigenvectors of the decay matrix as in the example above. One may then extrapolate exponentially for rather considerable time-steps until the nonlinearity of the decay requires local rediagonalization of the decay matrix.

Several techniques for handling stiff equations efficiently have been developed,[55-57] and generally the development has been oriented toward a particular type of problem, such as chemical reactive gas flow[55,57] and electrical circuit design. Gear[58,59] has written a versatile and efficient subroutine package that we have found to be extremely useful for integrating our system. A brief description of this routine is given here; more details, including a program listing, can be found in Gear.[58,59] The background theory of stiff equations solution techniques is discussed in Gear[60] and in literature cited therein. For handling stiff equations, the program was a modified predictor-corrector scheme in which the standard corrector iteration procedure is replaced by a Newton-Raphson iteration

scheme, which uses values of the elements of the Jacobian matrix. A subroutine that calculates these matrix elements and a matrix inversion routine are needed. A physical way of interpreting the technique is to consider it as a method of locally uncoupling the equation system, permitting large errors in the components that have decayed to insignificant concentrations and thus enabling large step-sizes to be taken.

Among other useful features of the program are automatic step-size control (depending on an error control parameter specified by the user) and variable integration order. The system takes the first step using a single-order predictor-corrector formula (then it is self-starting) and then automatically adjusts the order (up to maximum of six) to maximize the step-size.

Typically the program takes less than 12 sec of execution time on a CDC 6400 computer for a run involving 10 components and 32 reactions. The remarkable step-size increase made possible is illustrated by noting that for a 5000-nsec run the average step-size at any particular time is roughly 1/10 the sum of all previous integration steps. Thus after 1000 nsec have elapsed, step-sizes of 100 nsec are taken. Initially during the e-beam excitation period, however, the equations are not of the stiff type, and this method is no better than a standard Runge-Kutta scheme.

In Figures 12 and 13 we show typical computer model predictions for the kinetically important species over the experimentally accessible time range for two total pressures and mixture compositions. These plots conveniently illustrate the time scales of the various production and loss processes. The dominant energy pathway, $Ar^* \rightarrow N_2(B,C) \rightarrow N_2(A) \rightarrow NO(A)$, is easily identified.

The Ar^+ atomic ions (not shown) disappear very rapidly to form Ar_2^+. The decay of the diatomic ion is principally through recombination with electrons. The recombination is initially rapid but slows down as the electron density decreases. The Ar^* metastable atoms produced by this

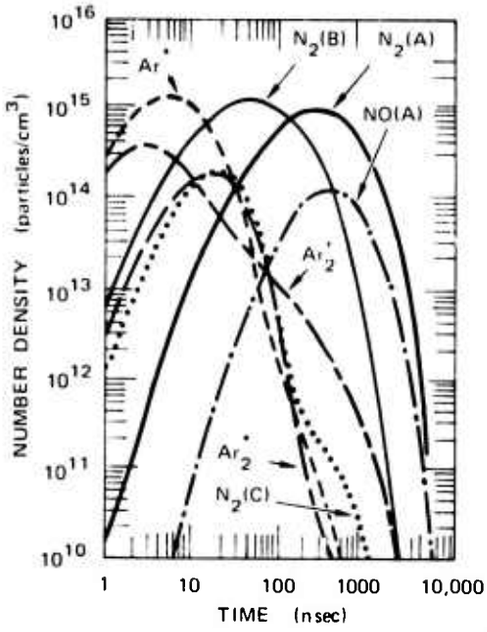

SA-1925-73R

FIGURE 12 MODEL PREDICTIONS OF THE TEMPORAL BEHAVIOR OF THE VARIOUS SPECIES IN THE EXCITED MIXTURE 95% Ar + 5% N_2 + 0.05% NO, AT 1550 torr TOTAL PRESSURE

The energy deposition source term is 2.28×10^{15} ions and metastables/cm^3.

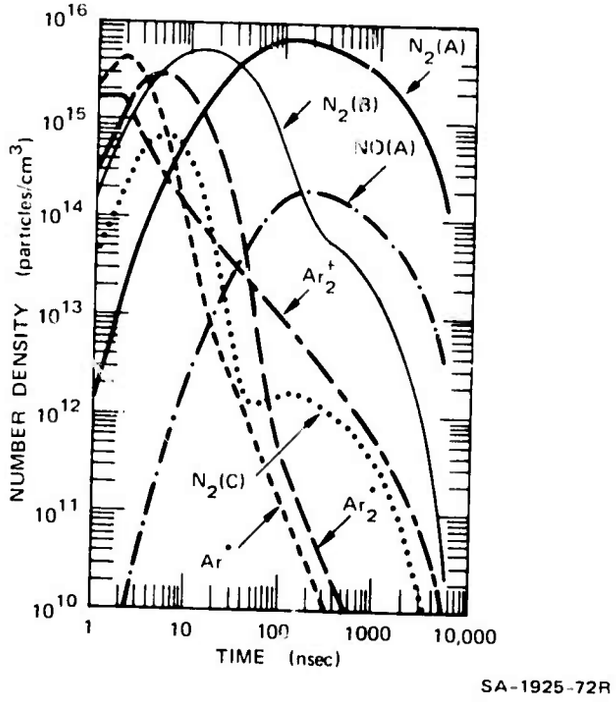

FIGURE 13 MODEL PREDICTIONS FOR THE MIXTURE 95% Ar + 5% N_2 + 0.005% NO AT 6100 torr

The source term is 9.30×10^{15} ions and metastables/cm^3.

recombination are converted to the Ar_2^* excimer or are quenched by N_2. The excimer then radiates or transfers to N_2.

The $N_2(C)$ peaks early in time and then decays rapidly because of the high quenching, [k_{15} and k_{16}]. After the initial decay, a shoulder or secondary maximum in the curve is produced by the pooling reaction [k_{22}], producing $N_2(C)$ states by $N_2(A)$-$N_2(A)$ collisions. The $N_2(B)$ state decays more slowly but also shows the regeneration by pooling reactions at late times. It is important to note that the model calculations predict that the $N_2(B)$ density should exceed that of $N_2(C)$ during all the stages of afterglow decay. The 2+(0-0) transition at 3371 Å will never be inverted. Our experimental results above showed that the $N_2(B)_{v=1}$ is much smaller (by a factor of 50-80) than $N_2(B)_{v=0}$. Hence laser action is expected on the transitions 2+(0-1) at 3577 Å and 2+(0-2) at 3805 Å. Our model could be improved to describe the different vibrational levels individually. The $N_2(A)$ and NO(A) states follow each other with a fixed density ratio, the decay of both states ultimately being determined by the energy transfer from $N_2(A)$ into NO(A). Although it is not clear from these figures, the final decay rates of the $N_2(B)$ and $N_2(C)$ states are twice that of $N_2(A)$.

Figures 14, 15, and 16 are comparison plots of the experimentally determined number densities and those predicted by the model calculations. The initial poor agreement between the calculations and experiments helped direct the research effort to identify and study the missing important reactions and to determine appropriate values of the rate coefficients.

One of the next improvements that should be included in our computer modeling will be to account separately for a few of the vibrational levels that appear to be specially important. The need for this has in fact been brought to light by the comparison between experimental and modeling results that we have carried out.

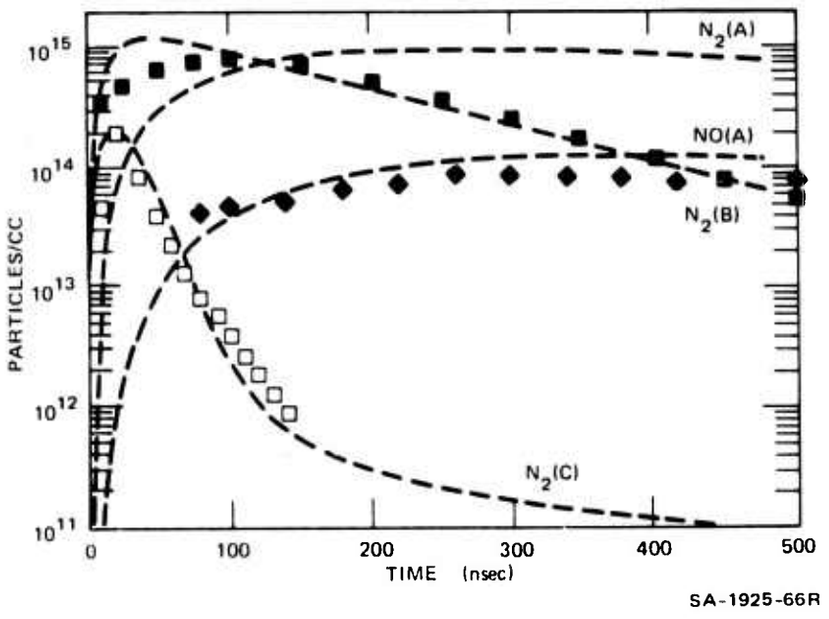

(a) 0.05% NO, 1550 torr TOTAL PRESSURE

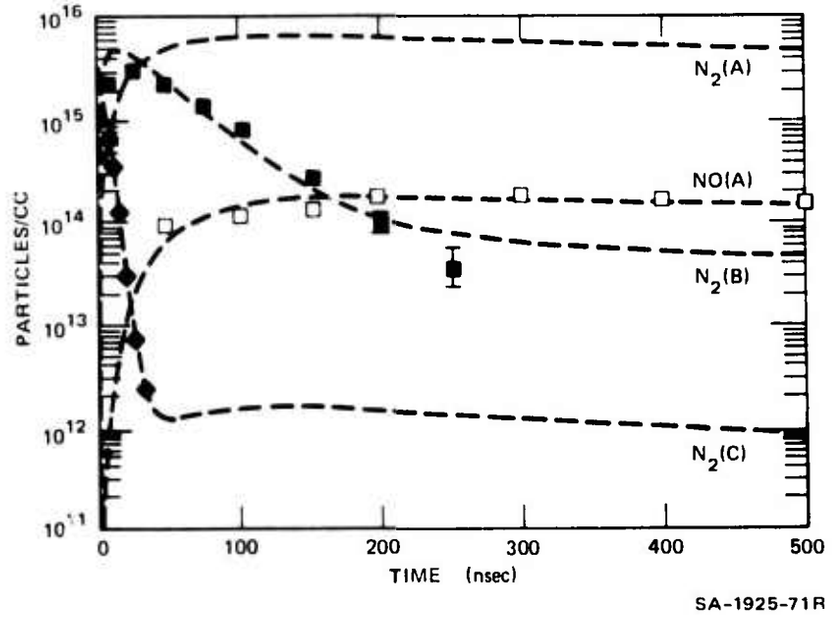

(b) 0.005% NO, 6100 torr TOTAL PRESSURE

FIGURE 14 COMPARISON OF MODEL PREDICTIONS WITH EXPERIMENTALLY MEASURED POPULATIONS FOR A MIXTURE OF 95% Ar + 5% N_2 + x% NO AT TWO TOTAL PRESSURES

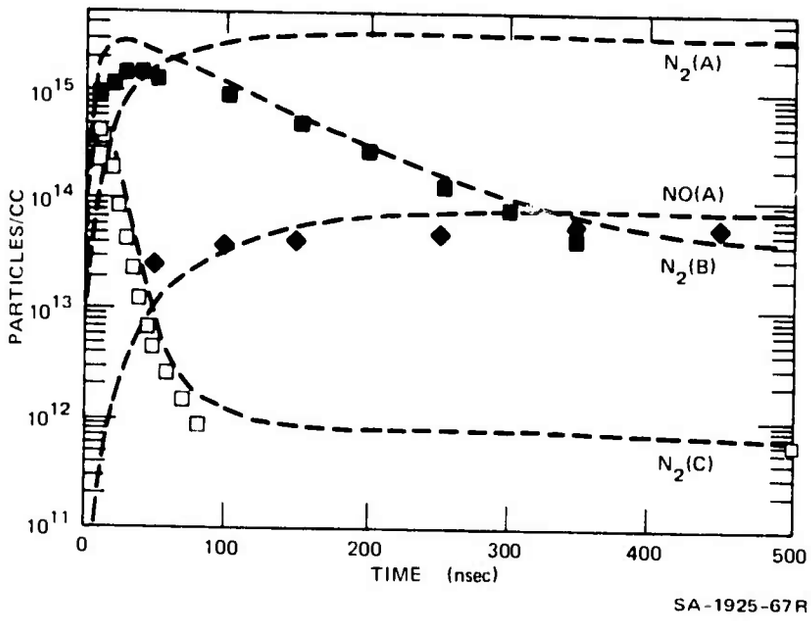

(a) 0.005% NO

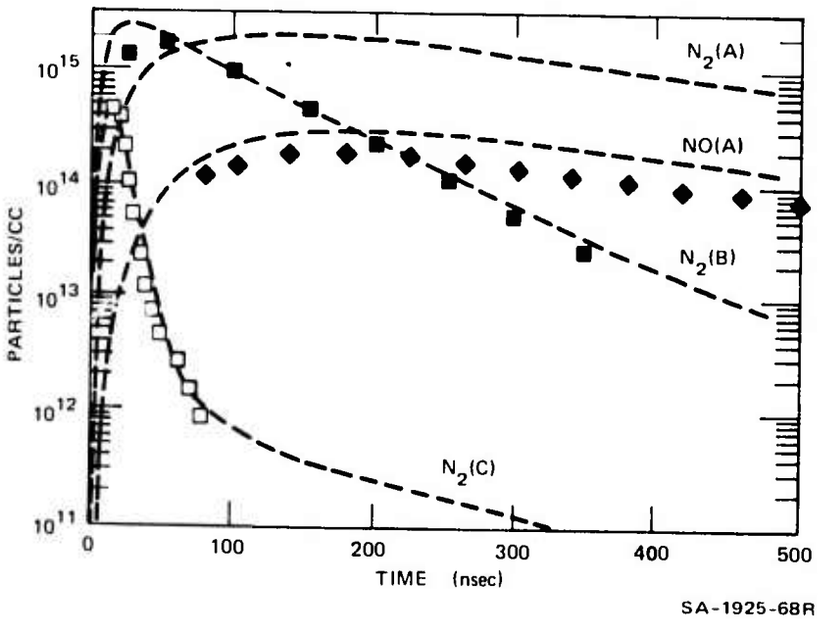

(b) 0.05% NO

FIGURE 15 COMPARISON OF MODEL PREDICTIONS WITH EXPERIMENTALLY MEASURED POPULATIONS FOR THE MIXTURE 95% Ar + 5% N_2 + x% NO AT 3100 torr TOTAL PRESSURE

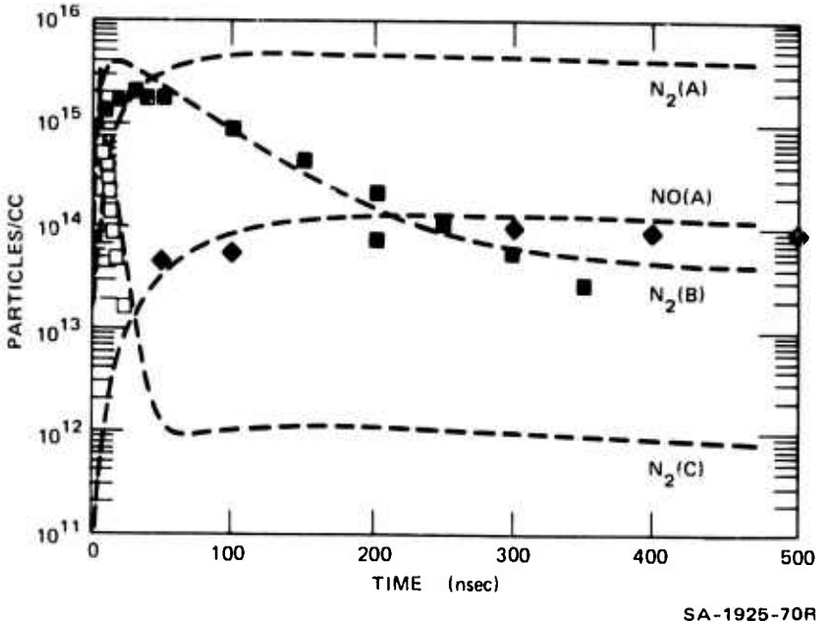

(a) 0.005% NO

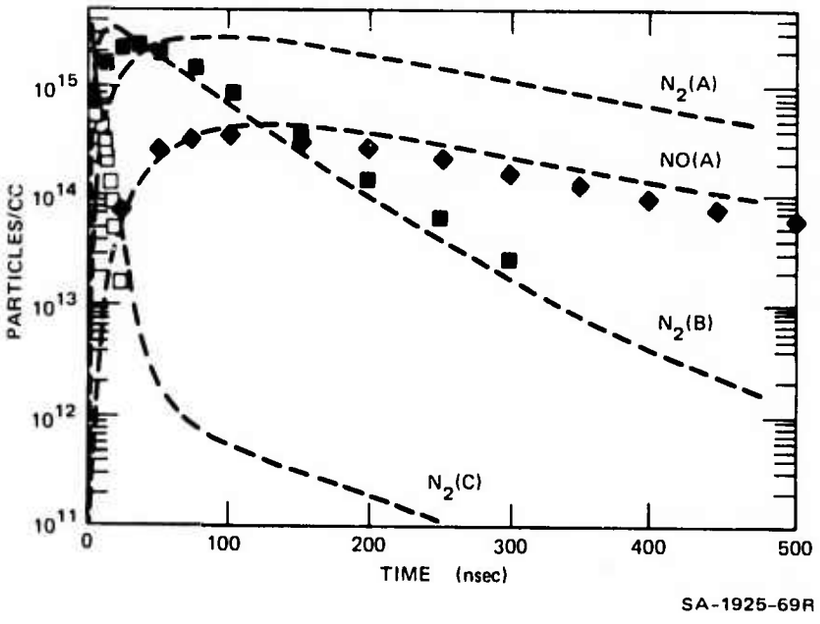

(b) 0.05% NO

FIGURE 16 MODEL PREDICTIONS AND EXPERIMENTAL POPULATIONS FOR Ar + 5% N_2 + x% NO AT 4650 torr

POSSIBLE LASER EFFICIENCY

Our kinetic model allows us to make predictions that can guide successful laser development. We can predict the "efficiencies" with which various excited states of acceptor gases can be produced and find the optimum gas densities and additive concentrations. In addition, we can estimate laser efficiencies for these optimum excitation conditions. In this section we give an estimate of a "probable" efficiency based on our own results and a "best possible" estimate based on overcoming the quenching problems in the upper and lower laser state.

We define peak population efficiency as the ratio of the peak population achieved in a particular state to the total production of atomic ions and metastable atoms, represented by the "source" term in our kinetic model. If this peak population is near the lasing threshold and if we presume that the lower level of the transition is initially empty but fills by lasing and therefore bottlenecks the transition, then an approximate value for the laser energy efficiency (eff) is given by

$$\text{laser eff} = (\text{rare gas pumping eff}) \times (\text{quantum eff}) \times (\text{peak population/source term}). \tag{12}$$

This is the minimum efficiency we would expect from the system.

We have seen that the $N_2(B)$ state quenches more slowly than the $N_2(C)$ and that the $N_2(A)$ state quenches more slowly than the $N_2(B)$ state. Thus, for both the 2+ and 1+ transitions, the lower state will tend to bottleneck, and only half of the peak population will be usable in a laser pulse. Obviously it would be useful to find ways to reduce the bottlenecking problems. In the Vegard-Kaplan system, the lower level of the lasing transition would be one of the higher vibrational levels of the ground state ($v'' = 5$-10); here bottlenecking might be eliminated by

vibrational relaxation of the ground state. For the NO γ-bands, the vibrational population in the ground state is certain to pose problems. An inversion has not yet been verified.

The quantum efficiency is the ratio of the energy of the 1+, 2+, V-K, or γ quantum to the 10 eV energy of the argon excimer. For purposes of discussion we will use 50% as the efficiency with which the e-beam pump energy can be converted into argon excimers.

In Figures 17 through 20 we show the peak population efficiencies for the various excited states of N_2 and for the NO(A) state from our kinetic model calculations. The maximum efficiencies range from about 10% for $N_2(C)$ and NO(A) to 65% for $N_2(B)$ and greater than 90% for $N_2(A)$. The low value for the $N_2(C)$ state is the result of the unfavorable branching ratio for transfer from the argon metastables and the high quenching of this state by both argon and N_2. $N_2(B)$ can be populated with much higher relative efficiencies, $\sim$ 60% to 65% for 10% N_2, because of its higher transfer efficiency and lower quenching. As we have already seen, almost all the excitation eventually finds its way to the $N_2(A)$ state. Because of its very low quenching and overall metastability, the $N_2(A)$ state has a population efficiency that exceeds 90% for 20% N_2.

NO is much less efficient as an energy acceptor. In the first place, the NO(A) state is very rapidly quenched by NO(X). In addition, NO interferes with the energy flow kinetics in the rare gas host. The NO ground state is ionized in collisions with Ar^+, Ar_2^+, Ar^*, and Ar_2^*. The resulting NO^+ then recombines with an electron to produce N and O atoms. At large NO concentrations ($\sim$ 0.1%), as much as 25% of the deposited energy can be consumed by these wasteful reactions.

Table V lists the estimated efficiencies for the possible laser transitions. The efficiency from peak population was calculated using equation (12), assuming complete bottlenecking. Since the most of the population in both $N_2(C)$ and $N_2(B)$ are in the v=0 vibrational levels, we

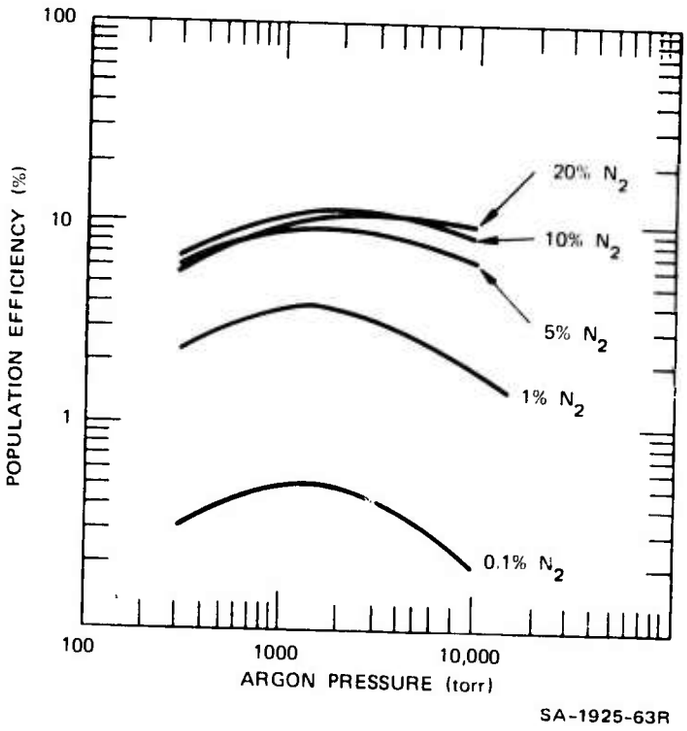

FIGURE 17 PEAK POPULATION EFFICIENCY OF $N_2(C)$ VERSUS ARGON PRESSURE

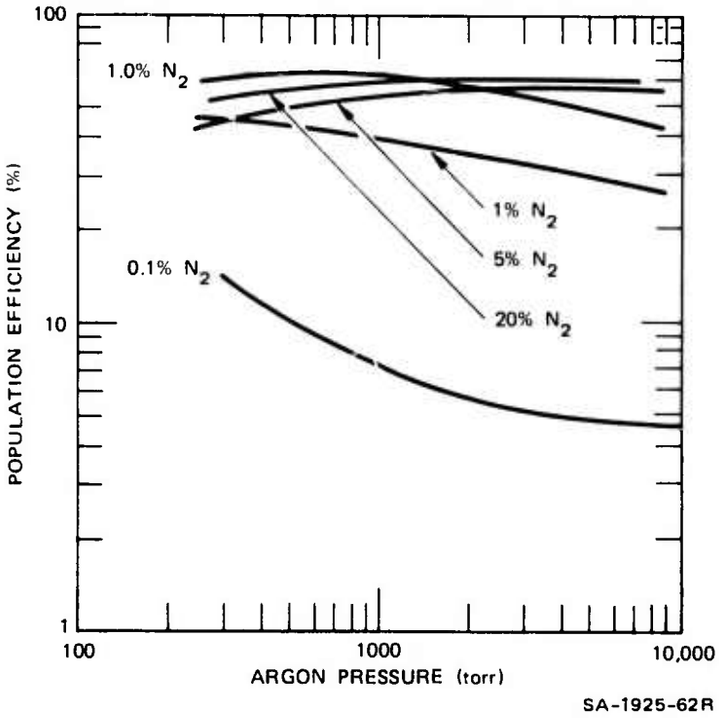

FIGURE 18 PEAK POPULATION EFFICIENCY OF $N_2(B)$ VERSUS ARGON PRESSURE

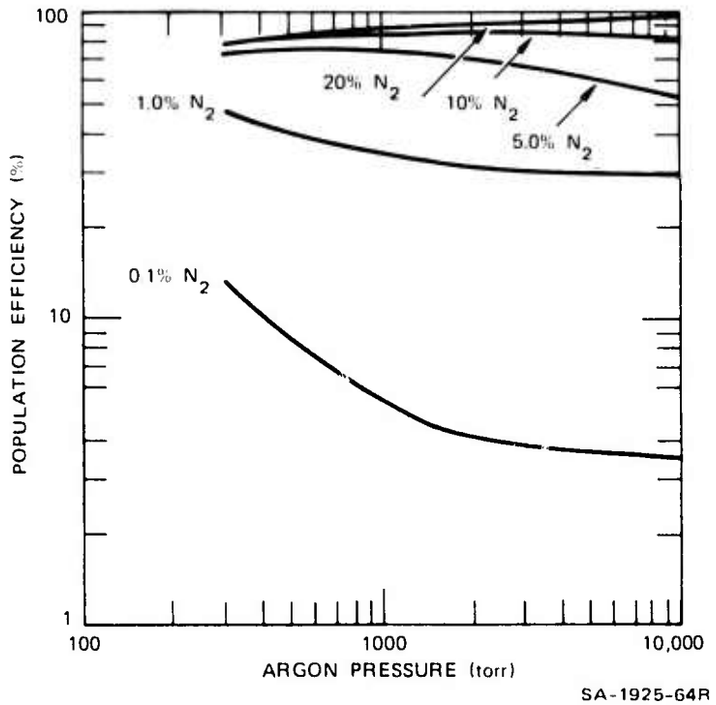

FIGURE 19 PEAK POPULATION EFFICIENCY OF $N_2(A)$ VERSUS ARGON PRESSURE

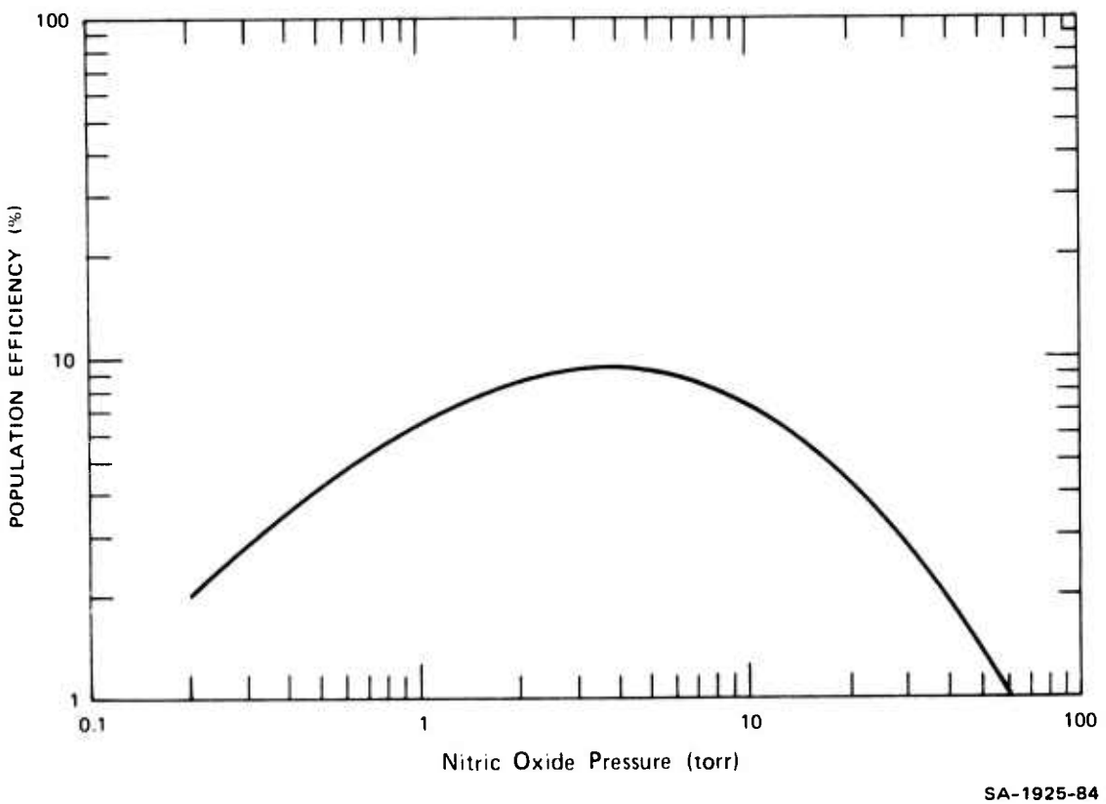

FIGURE 20 PEAK POPULATION EFFICIENCY OF NO($A^2\Sigma^+$) VERSUS NO(X) PRESSURE FOR 4200 torr Ar AND 450 torr N_2

Table V

POTENTIAL LASER EFFICIENCY

Upper State	Band System	Threshold Population[a]	Probable Transition	λ (Å)	Efficiency from Peak Population[b]	Efficiency from Total Production[c]
$N_2(C^3\Pi_u)$	2+	2.2×10^{13}	0-1 0-2	3577 3805	1%	8%
$N_2(B^3\Pi_g)$	1+	7.7×10^{13}	0-0	10,469	1.8%	6%
$N_2(A^3\Sigma_u^+)$	V-K	4.3×10^{17}[d]	0-5 to 0-7 1-8 to 1-10	2603 to 2935 2997 to 3424	11%	24%
$NO(A^2\Sigma^+)$	Y	7×10^{14}	0-1 to 0-5	2362 to 2848	1.3%	21%

(a) Assuming 0.01/cm gain, $\lambda/\Delta\lambda = 10^3$

(b) From equation (13)

(c) From equation (14)

(d) $N_2(A)$ transition probability = 10^3/sec

expect to see transitions only from those levels. Since the $N_2(B)$ v=0 is always greater than $N_2(C)$ v=0, we further expect that laser transitions in the 2+ will occur only on 0-1 or 0-2 bands. The listed threshold density values N_{th} were calculated using the gain equation

$$G = \frac{\lambda^3}{8\pi c} \frac{\lambda}{\Delta\lambda} (N_{th})A(v',v'') \qquad (13)$$

where we have used a gain of 0.01 per cm and $\lambda/\Delta\lambda$ of 10^3, which seem to be an appropriately conservative values for our conditions. $A(v',v'')$ is the spontaneous transition probability between the upper v′ vibrational level and the lower v″ level.

Several experimental observations of second positive laser radiation in electron beam pumped argon-nitrogen mixtures fit these predictions rather well.[27,29] The laser transitions are the 0-1 and 0-2, and the efficiencies observed range from 0.2 to 0.6%.

A second measure of the efficiency of the energy transfer scheme is provided by a calculation of the total production of the laser candidate. The peak population discussed above includes the competition between production and quenching losses. The intense laser field will shorten the effective radiative lifetime of the lasing state, making upper state quenching much less of a problem. It will still be necessary to remove the lower state bottlenecking. Just as the peak population efficiency provides a lower limit to the attainable efficiency, the total production efficiency provides an upper limit. The computed efficiencies

$$\text{laser eff} = (\text{rare gas eff}) \times (\text{quantum eff}) \times (\text{total species production/source term}) \qquad (14)$$

are shown in Table V.

We have seen that the $N_2(C^3\Pi_u)$ state is populated principally by direct energy transfer from excited argon atoms. The energy pooling

reaction of $N_2(A)$ will not be an effective method of producing 2+ radiation or a 2+ laser. The principal development problem remaining is the discovery of a quencher that will remove the bottlenecking lower state $N_2(B^3\Pi_g)_{v=1}$ or $N_2(B^3\Pi_g)_{v=2}$ without quenching the upper state. Pending the solution of this difficult problem, the maximum attainable energy efficiency should remain near 1%.

The $N_2(B^3\Pi_g)$ state also appears to be a promising laser candidate, although lasing action has not yet been demonstrated. Once again our studies indicate the principal production source to be transfer from excited argon atoms with a minor contribution from argon excimers. The possibility of significant production by $N_2(A)$ energy pooling is more remote but needs more study before it can be excluded. Improvement of the laser efficiency beyond the predicted 1.8% awaits the discovery of a quencher for $N_2(A^3\Sigma_u^+)_{v=0,1,2}$ that does not quench $N_2(B)$.

Table V shows the remarkable efficiency of $N_2(A^3\Sigma_u^+)$ as an energy acceptor and storage reservoir. Practical utilization of these excellent properties is made more speculative by the extremely small stimulated emission cross section. Indeed, the threshold density listed in Table V was determined by assuming that we could achieve a radiative transition probability of the order of 10^3/sec, or a 1000-fold larger than that observed for the free molecule. Just such a 1000-fold increase has been observed in the Vegard-Kaplan emissions of matrix isolated nitrogen in xenon.[61] If a similar enhancement could be achieved for the electron beam pumped case (say, in liquid xenon), efficiencies of 11-22% might be possible. The higher percentage presumes the use of all the peak $N_2(A)$ population, since the expected quenching of the vibrational levels in the ground electronic state of nitrogen would be fairly rapid.

As described above, the development of NO γ-band laser is inhibited by intrinsic difficulties in NO as an energy acceptor. Quenching of NO(A) by NO(X) is very rapid, and NO interferes with the argon energy

flow kinetics. The $NO(A^2\Sigma^+)_{v=0}$ is connected by large Franck-Condon factors with the lower vibrational levels of the ground state. It is not known to what extent these vibrational levels are populated by electron-excitation, v-v transfer from N_2, or NO quenching of NO(A). It will take careful study to even verify an inversion.

CONCLUSIONS

The spectral emission eminating from high pressure gas mixtures of Ar + N_2 + NO excited by energetic electron beams have been examined photographically and photometrically. The results are:

1. The excitation energy of the electron beam, initially deposited in the argon, is rapidly and efficiently transferred (via both the Ar metastable and the Ar_2 excimer) to the nitrogen triplet states.

2. The 14 reaction rate coefficients which we have measured for this system (see Table IV) with few exceptions agree well with those numbers already available in the literature.

3. The kinetic numerical model which describes the complex interaction of the excited gases (through 32 reaction equations) gives a reasonably accurate quantitative description of the experimental results.

4. The kinetic model predicts the potential laser efficiencies of $N_2(C)$ to be 1%, of $N_2(B)$ to be 1.8%, and of $N_2(A)$ to be 11%.

5. The high efficiency of conversion of electrical energy into excited electronic states of the rare gases (50%) coupled with the very high population efficiency of the $N_2(A)$ state (90%) produces large populations of metastable $N_2(A)$, and in fact indicates that this state has a long-lived high energy storage capacity.

REFERENCES

1. H. A. Koehler, L. J. Ferderber, D. L. Redhead, and P. J. Ebert, Appl. Phys. Letters 21, 198 (1972).

2. P. W. Hoff, J. C. Swingle, and C. K. Rhodes, Optics Comm. 8, 128 (1973).

3. P. W. Hoff, J. C. Swingle, and C. K. Rhodes, Appl. Phys. Letters 23, 245 (1973).

4. J. B. Gerardo and A. W. Johnson, J. Quant. Electr. QE-9, 748 (1973); J. Appl. Phys. 44, 4120 (1973).

5. D. C. Lorents and R. E. Olson, "Excimer Formation and Decay Processes In Rare Gases," Semiannual Technical Report No. 1, Contract N00014-72-C-0457, SRI Project 2018, Stanford Research Institute, Menlo Park, California, December 1972.

6. Franck Collier and Christian Collet, Bull. Am. Phys. Soc. 19, 156 (1974).

7. D. C. Lorents, D. J. Eckstrom, and D. L. Huestis, "Excimer Formation and Decay Processes in Rare Gases," Final Report, Contract N00014-72-C-0457, SRI Project 2018, Stanford Research Institute, Menlo Park, California, September 1973.

8. a. E. V. George and C. K. Rhodes, Appl. Phys. Letters 23, 139 (1973);
   b. P. W. Hoff, J. C. Swingle, C. K. Rhodes, C. W. Werner, and E. V. George, VIII International Quantum Electronics Conference, San Francisco, June 1974.

9. H. A. Koehler, L. J. Ferderber, D. L. Redhead, and P. J. Ebert, Phys. Rev. A9, 768 (1974).

10. D. W. Setser, D. H. Stedman, and J. A. Coxon, J. Chem. Phys. 53, 1004 (1970).

11. L. G. Piper, W. C. Richardson, G. W. Taylor, and D. W. Setser, Discussions Faraday Soc. 53, 100 (1972).

12. D. J. Eckstrom, R. A. Gutcheck, R. M. Hill, D. Huestis, and D. C. Lorents, "Studies of E-Beam Pumped Molecular Lasers," Semiannual Technical Report No. 2, Contract N00014-72-C-0478, SRI Project 1925, Stanford Research Institute, Menlo Park, California, July 1973.

13. S. K. Searles and G. A. Hart, Appl. Phys. Letters 25, 79 (1974).

14. E. R. Ault, M. L. Bhaumik, and N. T. Olson, "High Power Ar-N_2 Transfer Laser at 3577," to be published in IEEE J. Quant. Electr.

15. M. J. Mumma and E. C. Zipf, J. Opt. Soc. Am. 61, 83 (1971).

16. E. W. McDaniel, V. Cermak, A. Dalgarno, E. E. Ferguson and L. Freidman, Ion-Molecule Reactions (Wiley-Interscience, New York, 1970), p. 338.

17. J. N. Bardsley and M. A. Biondi, Advances in Atomic and Molecular Physics (Academic Press, New Yor, 1970), Chap. I.

18. E. Ellis and N. D. Twiddy, J. Phys. B 2, 1366 (1969).

19. J. LeCalvé and M. Bourene, J. Chem. Phys. 58, 1446 (1973).

20. R. A. Gutcheck and E. C. Zipf, Bull. Am. Phys. Soc. 17, 395 (1972).

21. H. A. Koehler, Lawrence Livermore Laboratory (private communication).

22. L. G. Piper, J. E. Velazco, and D. W. Setser, J. Chem. Phys. 59, 3323 (1973).

23. M. Bourene and J. LeCalvé, J. Chem. Phys. 58, 1452 (1973).

24. J. M. Calo and R. C. Axtmann, J. Chem. Phys. 54, 4961 (1971).

25. J. M. Calo and R. C. Axtmann, J. Chem. Phys. 54, 1332 (1971).

26. J. E. Hesser, J. Chem. Phys. 58, 2518 (1968).

27. M. Jeunehomme and A.B.F. Duncan, J. Chem. Phys. 41, 1692 (1964).

28. A. W. Johnson and R. G. Fowler, J. Chem. Phys. 53, 65 (1970).

29. P. Millet, Y. Salamero, H. Brunet, J. Galy, D. Blanc, and J. L. Teussier, J. Chem. Phys. 58, 5839 (1973).

30. M. Jeunehomme, J. Chem. Phys. 45, 1805 (1966).

31. D. E. Shemansky and A. W. Jones, Planet. Space Sci. 16, 1115 (1968).

32. D. C. Shemansky and A. L. Broadfoot, J. Quant. Spectros. Rad. Trans. 11, 1385 (1971).

33. J. W. Dreyer and D. Perner, Chem. Phys. Letters 16, 169 (1972).

34. R. A. Young, G. Black, and T. G. Slanger, J. Chem. Phys. 50, 303 (1969).

35. W. Brennan and E. C. Shane, Chem. Phys. Letters 2, 143 (1968).

36. G. N. Hays and H. J. Oskam, J. Chem. Phys. 59, 1507 (1973).

37. G. N. Hays and H. J. Oskam, J. Chem. Phys. 59, 6088 (1973).

38. E. C. Zipf (private communication).

39. D. H. Stedman and D. W. Setser, J. Chem. Phys. 50, 2256 (1969).

40. E. C. Zipf, Bull. Am. Phys. Soc. 10, 179 (1965).

41. E. E. Ferguson (private communication); D. K. Bohme, N. G. Adams, M. Mosesman, D. B. Dunkin, and F. C. Fehsenfeld, J. Chem. Phys. 52, 5094 (1970).

42. A. B. Callear and P. M. Wood, Trans. Faraday Soc. 67, 272 (1971).

43. R. A. Young and G. A. St. John, J. Chem. Phys. 48, 895, 898 (1968).

44. A. B. Callear and I.W.M. Smith, Trans. Faraday Soc. 59, 1720 (1963).

45. R. W. Nicholls, Ann. Geophys. 20, 144 (1964).

46. M. Jeunehomme, J. Chem. Phys. 45, 4433 (1966).

47. H. Bubert and F. W. Frolen, Chem. Phys. Letters 8, 242 (1971).

48. H. P. Broida and T. Carrington, J. Chem. Phys. 38, 136 (1963).

49. L. A. Melton and W. Klemperer, J. Chem. Phys. 59, 1099 (1973).

50. A. B. Callear and M. J. Pilling, Trans. Faraday Soc. 66, 1618 (1970).

51. G. S. Hurst (private communication).

52. J. W. Dreyer and D. Perner, J. Chem. Phys. 58, 1195 (1973).

53. W. Brennen, R. V. Gutowski, and E. C. Shane, paper FD4, "Energy Transfer in the $A^3\Sigma_u^+$ State of Nitrogen," presented at the 29th Symposium on Molecular Structure and Spectroscopy, Ohio State University, Columbus, Ohio, June 10-14, 1974.

54. D. C. Lorents, R. M. Hill, and D. J. Eckstrom, "Molecular Metal Lasers," Final Report, Contract N00014-72-C-0478, SRI Project 1925, Stanford Research Institute, Menlo Park, California, November 1972.

55. C. E. Treavor, Math. Comp. 20, 39 (1966).

56. I. W. Sandberg and H. Shichman, Bell System Tech. J. 46, 1243 (1967).

57. H. E. Bailey, Phys. Fluids 12, 2292 (1969).

58. C. W. Gear, Comm. ACM 14, 176 (1971).

59. C. W. Gear, Comm. ACM 14, 185 (1971).

60. C. W. Gear, Numerical Initial Value Problems in Ordinary Differential Equations, Chap. 11 (Prentice-Hall, Inc., Englewood Cliffs, New Jersey, 1971).

61. D. S. Tinti and G. W. Robinson, J. Chem. Phys. 49, 3229 (1968).